A review of chloride-induced steel corrosion in coastal reinforced concrete structures: Influence of micro-climate

Chandra Sekhar Das[1], Zheng Haibing[2,*], Jian-Guo Dai[3,*]

1. Department of Civil and Environmental Engineering, The Hong Kong Polytechnic University, Hong Kong.
2. Institute of Chemistry, Henan Academy of Sciences, Zhengzhou, 450046, China.
3. Department of Architecture and Civil Engineering, City University of Hong Kong, Hong Kong.

*** Corresponding author:**

Haibing Zheng, Email: zhenghaibing.ln@163.com

Jian-Guo Dai, Email: jiangdai@cityu.edu.hk

Abstract

The corrosion initiation by chlorides for reinforced concrete (RC) structures is influenced by the nature of chloride transport through concrete and the chloride threshold. These two properties vary with the chloride exposure conditions and concrete properties. Since most lab-scale experiments are conducted for isolated exposure cases under controlled conditions, the coupling effect of micro-climate, such as temperature, wind features, carbon dioxide ingress, wet/dry cycle durations, and rainfall, on corrosion initiation is not thoroughly discussed. This review addresses the role of micro-climate in both chloride transport and chloride threshold for corrosion initiation in different marine exposure zones. The mechanism of coupled interactions and the influence of concrete mixes are discussed. The review emphasises the need to standardize chloride-induced corrosion experiments that consider micro-climate conditions to ensure the comparability of data. A limited understanding of chloride-induced steel corrosion risk is evident in alternative binders that have recently been developed. Finally, the review provides future research directions to clarify some coupled interactions that have not been well understood.

Keywords: Reinforced concrete; Steel Corrosion; Micro-climate; Chloride transport; Chloride threshold

1. Introduction

The primary cause of early-age deterioration in coastal reinforced concrete (RC) structures is reinforcement corrosion, which is triggered by the accumulation of chloride ions at the steel surface beyond a certain threshold (Angst et al., 2009; Ann and Song, 2007; Cao et al., 2019). Even in cases where carbonation proceeds simultaneously with chloride ingress, previous studies indicate that in coastal areas, carbonation is slower than chloride transport (Kuosa et al., 2014; Liu et al., 2016a; Qiu, 2020; Yoon, 2007), making chlorides the leading factor behind corrosion. This is due to the ability of chlorides to partially clog the concrete pores and retain moisture, leading to increased pore relative humidity (Malheiro et al., 2021). However, the progress of the carbonation front changes the chloride distribution in concrete. Gradually, as chlorides accumulate at the steel surface, it causes the breakdown of the passive film and depassivation of the steel. Due to a thick concrete cover, chlorides take several years to reach the steel surface and start corrosion. The time to depassivation is known as the corrosion initiation time and is crucial in assessing the structure's long-term serviceability against corrosion.

Structures in different regions are constantly exposed to the natural climate, which varies globally across diverse climate zones characterized by factors such as humidity, temperature, and salt concentrations in the oceans. These climate zones often have sub-classifications that further define the specific characteristics of a region's climate, marked by annual, seasonal, and daily fluctuations. Even in the same area, the structure's orientation and local modification brought by construction and rapid development create urban heat islands and alter wind patterns, leading to distinct micro-climate conditions for different structural elements. It has been observed that micro-climate conditions tend to cause a great degree of variation in chloride distribution even for the same structure (Costa and Appleton, 1999) and also corrosion current density (El Hassan et al., 2010; Jaśniok and Jaśniok, 2015) leading to varying levels of corrosion severity by chlorides.

Many studies have shown that these distinct micro-climate conditions can significantly impact the long-term corrosion-induced damage caused by chlorides. For instance, during an inspection of 879 RC piles for the Hornibrook Bridge in Australia, extensive damage was found on the underside of bridge slabs,

while the piles remained in good condition after 75 years of service (Melchers et al., 2017). A similar situation occurred at a cooling tower in a thermal power station, which experienced severe deterioration in specific areas just three years into its 25-year design service life (Segura et al., 2016). Analysis revealed that the southeastern side of the structure, facing the sea, experienced accelerated corrosion initiation due to wetting and drying cycles. In a structure in Brazil, locations subjected to wetting and drying cycles of salt water suffered severe damage, with chloride contents about 3-8x of those locations without such cycles (Medeiros et al., 2013). Another case involved a chimney structure located in the Mediterranean region that had to undergo several cycles of repairs during 47 years of service due to the synergistic effect of chloride contents exceeding the threshold value at steel reinforcement and carbonation of concrete cover (Carsana et al., 2022).

While the cause of variations in chloride distribution and corrosion damage in concrete has been attributed to the micro-climate effect in many literature, the existing reviews have mainly focused on the evaluation of the durability of different concrete mixes, testing methodologies and protection methods in marine environments (Song et al., 2008); (Angst et al., 2009); (Shi et al., 2012); (Shafikhani and Chidiac, 2019; Zhang and Zhang, 2014); (Yi et al., 2020); (Liang et al., 2021). The current ways to assess corrosion risk due to chlorides in RC structures at laboratories rely on simplistic exposure schemes such as wet-dry cycles, sustained submergence in a salt solution, salt spray, accelerated carbonation, and chloride electromigration to simulate the conditions encountered in practice, which fails to capture the complex interplay between multiple controlling processes (Andrade et al., 2002; Lindvall, 2007). This becomes particularly relevant in light of the ongoing unprecedented climate change, which may lead to more uncertain events in the future.

Therefore, this research aims to provide an overview of how different micro-climates influence corrosion initiation in reinforcing steel due to chlorides. The corrosion initiation time has been presented to depend on the rate of chloride transport in concrete cover and the chloride threshold. First, we evaluate the critical micro-climate factors in different exposure zones. Then, we discuss the influence of critical micro-climate factors on chloride transport and chloride threshold. This is followed by identifying the limitations of current work and directions for future research. Finally, the review ends

with an overall summary of the findings. The outcome of this review would shed light on some coupled interactions that have not yet been well understood and enable the selection of suitable concrete mix to achieve maximum long-term serviceability against chloride-induced corrosion. It is worth noting that this study only considers the service environments of RC structures where corrosion risk due to chlorides is more than carbonation.

2. Critical micro-climate factors in different exposure zones

The chlorides accumulate on the surface of the RC structure either when they are in direct contact with seawater (as in port and offshore structures) or due to the winds carrying airborne chlorides (as for coastal buildings and bridges). Generally, the field data have shown that higher chloride deposits on a concrete surface increase its corrosion susceptibility (Meira et al., 2010; Meira et al., 2007b). For example, Meira et al. (Meira et al., 2010) found that when the chloride deposition rate increased from 120 mg/m^2.day to 500 mg/m^2.day, the structure's service life due to corrosion was shortened by about 30-60%. This surface chloride deposition rate varies by the structure's location (e.g., its height above sea level and distance from sea) such that as the structure location moves away from the sea, the chloride deposition drops significantly in the first 200 meters, followed by a gradual decrease after that. Based on the risk of corrosion by chlorides, RC structures are classified into different exposure zones: submerged zone, tidal zone, splash zone, and atmospheric zone.

The submerged zone represents the structures or a part of the structure which remains below sea level year-round. The chloride penetrates the concrete cover by diffusion due to the concentration gradient. However, the corrosion rate in this case is limited by dissolved oxygen seawater. Thus, the corrosion rate is generally low (Page, 1975). Only in some underwater tubular structures, such as tunnels, severe chloride-induced corrosion occurs by macrocell formation in zones with different aerations and can be quite severe (Pergola et al., 2013). The primary degradation mechanism for the concrete submerged inside seawater is a combined chemical attack by sulphate ions and other salts and physical weathering (Yi et al., 2020); (Santhanam and Otieno, 2016). Thus, the relevant micro-climate parameters in

97 submerged zones affecting chloride transport are the salinity of seawater (i.e., salt concentration) and
98 concentrations of other aggressive ions which can cause degradation in concrete.

99 The atmospheric zone refers to any part of a structure that is aerated throughout the year, including
100 coastal reinforced structures located within a few kilometres from the shore. In this zone, chlorides from
101 seawater can reach the structure in the form of airborne chlorides carried by winds. Due to the fully
102 aerated condition, there is easy access for gases such as oxygen and carbon dioxide to the steel surface.
103 The degree of pore saturation, which affects the chloride and gas transport rate, is primarily influenced
104 by micro-climate factors such as temperature, relative humidity and rainfall characteristics in
105 atmospheric zones.

106 The tidal and splash zones comprise any part of a structure that undergoes wetting and drying cycles
107 and are sometimes grouped (Yi et al., 2020). The tidal zone encompasses the area between high and
108 low tide levels of seawater, while the splash zone refers to the parts above the tidal zone that are exposed
109 to marine splashes. Due to their relatively higher elevation, the splash zone experiences longer drying
110 periods than the tidal zone. The drying and wetting periods are also influenced by local micro-climate
111 factors such as temperature, humidity, wind speed, and direction, which ultimately affect the nature of
112 chloride transport and the accessibility of gases into the concrete pores for tidal and splash zones.

113 The dominating climatic factors influencing chloride transport when exposed to different conditions
114 can be illustrated as shown in Fig. 1.

Fig. 1. Schematic of different exposure zones in a coastal RC structure and the critical micro-climate factors affecting chloride transport and chloride threshold in each zone

Once chlorides reach the steel surface, the transition from passive to active state depends on the chloride threshold and varies with the nature of aggressive ions and the concrete's internal environment. The internal concrete environment, such as moisture content in the pores, chemical composition of the pore solution and oxygen availability at the steel surface, are altered by micro-climatic factors such as exposed temperature, carbonation and relative humidity of the region or periods of drying and wetting seawater cycles (Andrade et al., 2002; Zhang et al., 2023a). These ultimately affect the chloride threshold value. Thus, the interaction between micro-climatic factors and the chloride threshold value is more indirect than the chloride transport process.

3. Effects of micro-climatic factors on chloride transport

3.1 Effect of wind

Winds primarily act as carriers for chloride ions from seawater to coastal structures in the atmospheric zone. The oceanic winds are rich in marine aerosols, comprising particles of sizes ranging from 0.1 to 400 μm. Among these particles, it has been observed that marine aerosol particles of size > 10 μm have the highest corrosivity impact (Ambler and Bain, 1955). However, with an increase in particle size, the

tendency of the particles to settle down (sediment) increases. In such situations, the ability of the wind to transport particles over large distances plays a key role in promoting corrosion. One key point observed is that a certain threshold wind speed exists beyond which the salt concentration increases steeply. This speed has been identified to vary between 3 m/s and 7.1 m/s in different studies (Meira et al., 2007a; Meira et al., 2008; Meira et al., 2006; Morcillo et al., 2000)., and the reason has been attributed to the increased number of salt particles and increased percentage of larger-sized particles at higher wind speeds.

An exponential growth function has been used to draw the relationship between salt concentration (D) and wind speed with time (t) (Meira et al., 2007a), as represented by Equation 1.

$$D = D_1 + ae^{b(\frac{3t_3}{t})} \quad (1)$$

where, a and b are constants influenced by location and local climatic conditions, D_1 is the chloride deposition by wind speeds less than 3 m/s, t_3 is the time length when wind speed was more than 3 m/s.

However, a previous study has pointed out that chloride deposition may hold more relevance to wind power, defined by the product of wind speed and the residence time (Feliu et al., 1999). For example, a high-intensity wind speed for a longer duration can significantly increase salt deposition. This is particularly evident during storms, which deposit large quantities of salt despite impacting for a few hours.

In addition to influencing surface chloride deposits, the winds influence chloride penetration in wet-dry cycles. A study performed in coastal regions of Northeast Brazil (de Medeiros-Junior et al., 2015) concluded that winds promoted faster drying of concrete surfaces for sidewalls subjected to cyclic wetting and drying. This moisture reduction in concrete created an imbalance that slowed the chloride penetration.

3.2 Effect of periodic drying and wetting

For offshore and port structures, the moisture condition in the concrete is significantly influenced by the wet-dry cycles due to marine splashes (Medeiros et al., 2013). Several laboratory studies and field

exposure results have demonstrated that the wet-dry periodic cycles in marine splash zones accelerate the chloride migration and change the chloride profile distribution in the concrete (Arya et al., 2014; Cai et al., 2020; Jin et al., 2022; Ju et al., 2021; Tongning et al., 2020; Ye et al., 2016; Zuquan et al., 2018). This causes the peak chloride concentration value to be obtained at a certain depth inside the concrete. This depth is termed as convection zone and mainly originates due to the coupling effect of convection and diffusion in the concrete surface layer.

When concrete subjected to marine splashes undergoes a drying period after wetting, water loss starts from the evaporation front (exposed surface of concrete) and proceeds inwards. Thus, depending on the drying period's length and the concrete's quality, only a certain depth of the concrete will undergo moisture loss (i.e., a decrease in the saturation degree) during the drying stage (Hong and Hooton, 1999). Typically, these depths range between 0-15 mm (Lu et al., 2015; Wu et al., 2023; Zhang et al., 2023b) and are formed due to the slower drying rate of concrete than its wetting (Spragg et al., 2011). Thus, these shallow concrete depths will have a high concentration of chlorides, which are later transported into the concrete depths in the subsequent wetting stage. Depending on the length of the drying period and degree of saturation in the near-surface regions, the chloride transport through this layer in the following wetting stages can be by capillary action or diffusion.

The time for the development of this convection zone is dependent on durations of wet and dry cycles. For example, the convection zone is only formed after a prolonged exposure period in concretes subjected to short dry/wet cyclic exposures but is more evident at a short exposure duration in concretes exposed to longer dry/wet cycles (Cao et al., 2022; Gang et al., 2015; Jin et al., 2023) (Fig 2(a)). This is because, in small dry/wet cycle exposure, concrete remains nearly saturated, thus leading to slower diffusion-based transport almost uniformly throughout the concrete. However, in the case of extended dry/wet cycles, the capillary action of chloride transport plays a dominating role in the near-surface concrete, followed by diffusion-based transport at greater depths. An increase in the number of wetting and drying cycles also increases the convection depth and the peak chloride concentration in the concrete (Cao et al., 2022; Chen et al., 2023). This is attributed to the moisture changes in the concrete until a greater depth and subsequent higher chloride ingress under capillary action. Notably, the

capillary-based absorption also varies with the chloride content in concrete (Xie et al., 2023). For example, at low chloride levels, water absorption is promoted due to the hygroscopic effect of salts. However, at higher chloride levels, the blockage of some of the pores by chlorides reduces water uptake.

The influence of concrete mix proportions on convection depth and peak chloride content is rather unclear from available studies. There seems to be a consensus that increasing porosity in concrete increases the convection depth and peak chloride, which is observed in samples with different w/b ratio where high w/b results in greater convection depth (Chang et al., 2017; Zhang et al., 2023b). However, the addition of SCMs has contradicting effects in available studies. Cao et al. (Cao et al., 2022) observed that adding FA and GGBS reduced peak chloride contents but had a negligible impact on convection depth. These results align with the trend in the study by Zhang et al. (Zhang et al., 2023b), who exposed 14 sample groups to natural and simulated environments and predicted the randomness of convection depth. Their study found that the random distribution in convection depth for short-term studies followed the same trend as natural long-term exposures. Moradllo et al. (Moradllo et al., 2018) observed that increasing silica fume dosage from 5% to 12.5% in concrete reduced the convection depth. On the contrary, experimental results from Lu et al. (Lu et al., 2015) demonstrated that increasing FA contents negatively affected concrete durability by increasing peak chloride contents and the convection depth (Fig. 2(b)). The detailed experimental conditions for studies by Cao et al. (Cao et al., 2022) and Lu et al. (Lu et al., 2015) are provided in Table 1 of the Appendix.

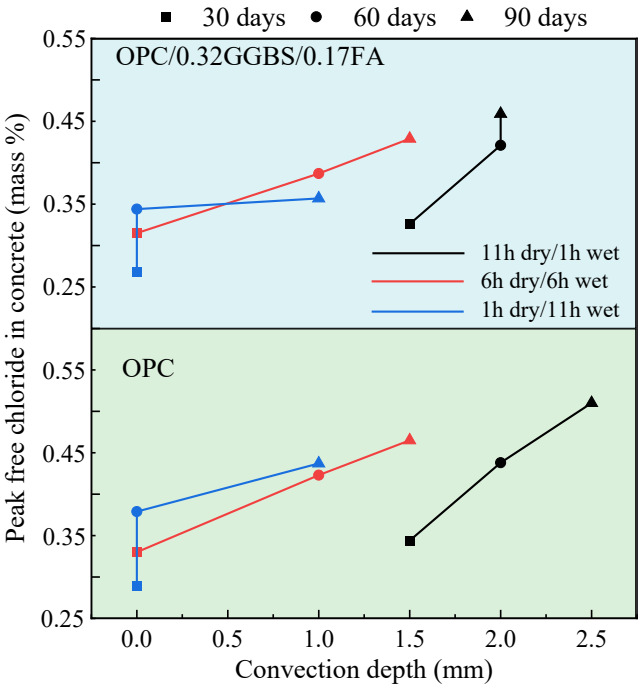

(a)

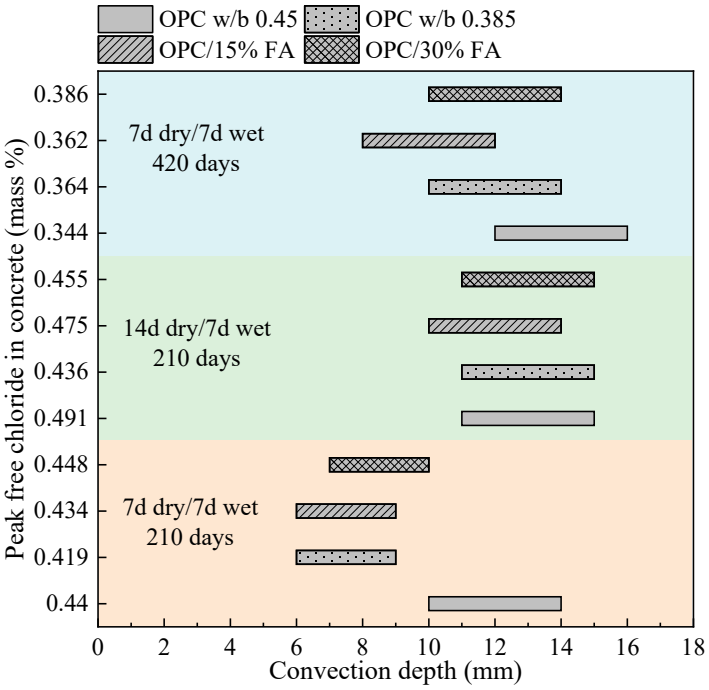

(b)

Fig. 2. Peak chloride concentration and convection depth in concretes subjected to different wet/dry periods observed in (a) data obtained from (Cao et al., 2022) and (b) data obtained from (Lu et al., 2015).

3.3 Effect of rainfall

While the moisture states of concrete in splash and tidal zones are governed by wetting and drying cycles, the RC structure in a coastal atmospheric zone is primarily influenced by the relative humidity and rainfall distribution (Andrade et al., 1999; Liu et al., 2018; Liu et al., 2016c; Medeiros-Junior, 2018). The exposure of unsheltered chloride-contaminated concrete structures (i.e., with airborne chloride deposits) has two effects: the rainwater washes off some chloride ions from the surface, and there is some rainwater absorption by concrete.

For completely saturated concrete, chloride transport from the surface to the inside of concrete occurs primarily by diffusion. Hence, the surface chloride content only decreases slightly for a shorter exposure. With the increase in exposure time, a convective zone is usually formed due to the higher erosion of chlorides from the concrete surface, as observed in marine splash zones. In contrast, for the unsaturated chloride-contaminated concrete exposed to rainwater, a convection zone and a decrease in surface chloride concentration occur even at a shorter exposure. This can be attributed to more rainwater absorption and chloride transport by capillary action.

For the same rainfall duration, this difference between surface and peak chloride concentration also increases with the increase in rainfall intensity, attributed to the higher kinetic energy of rain and subsequent damage to the surface (Jin et al., 2021). It has been reported that degradation due to high rainfall intensity also reduces the chloride binding capacity of concrete. This is a consequence of the deterioration of concrete pores and the subsequent release of chloride ions from Friedel's salt (Jin et al., 2021).

3.4 Effect of surrounding temperature

Generally, an RC structure is subjected to different temperatures due to daily and seasonal variations. The effect of service temperature on chloride transport can be explained in terms of 1) the chemical interaction between chloride ions and concrete; and 2) the transport rate of chlorides through concrete.

Chemical interaction between chloride ions and concrete

A significant part of chlorides entering the concrete gets bound to the hydration products (i.e., undergo chloride binding) and does not pose a corrosion risk in non-carbonated concrete (Florea and Brouwers, 2012). Thus, a greater chloride binding capacity of binders is usually preferred as it slows down the net chloride ingress (Li and Shao, 2014). It has been observed that when concretes are exposed to chlorides at different temperatures, there is an increase in free chloride as the temperature is increased in plain and blended Portland cement (Dousti and Shekarchi, 2015; Hussain, 1993; Maslehuddin et al., 1997; Panesar and Chidiac, 2011; Tran et al., 2021; Xu et al., 2016). However, some studies have pointed out that variation of chloride binding at different temperatures does not follow the same trend at different chloride concentrations (Ogirigbo and Black, 2017; Zibara, 2001). For example, the chloride binding reduces with temperature rise at lower chloride concentrations of 1 M or less. At high chloride concentrations, i.e., 3M, the chloride binding increases with increasing temperature. The variation arises due to different mechanisms controlling the binding at different temperatures. However, there seems to be no general consistency in both results and the mechanism governing chloride binding at different temperatures. Another important phenomenon is that the mix proportions also seem to affect the chloride binding changes at different temperatures. This could be observed in the bound chloride contents observed in equilibrium with 1 M free chlorides, as shown in Figure 3. However, the trend is not quite clear. It must also be noted that among the three studies compared ((Dousti and Shekarchi, 2015; Panesar and Chidiac, 2011)), even for the same mix of OPC, the observed chloride binding ability varies significantly in the study by Dousti and Shekarchi (Dousti and Shekarchi, 2015). This could be primarily linked to the higher curing age of 56 days in one study (Dousti and Shekarchi, 2015) compared to 28 days in the other two studies (Panesar and Chidiac, 2011); (Zibara, 2001). The detailed experimental conditions in are given in Table 2 of the Appendix.

In addition to chlorides, seawater contains a large concentration of sulphate ions, which penetrate the concrete along with chloride ions. It has been observed that the presence of sulphate ions reduces the amount of chloride getting bound to the hydration products. This is attributed to the preferential reaction of the sulphate over chloride ions with tricalcium aluminate (C_3A) to form calcium sulphoaluminate hydrate compounds (Dehwah et al., 2003; Maslehuddin et al., 1997). Thus, the presence of high chloride

and sulphate ions in the pore solution of binders at elevated temperatures can pose serious corrosion issues to the reinforcement.

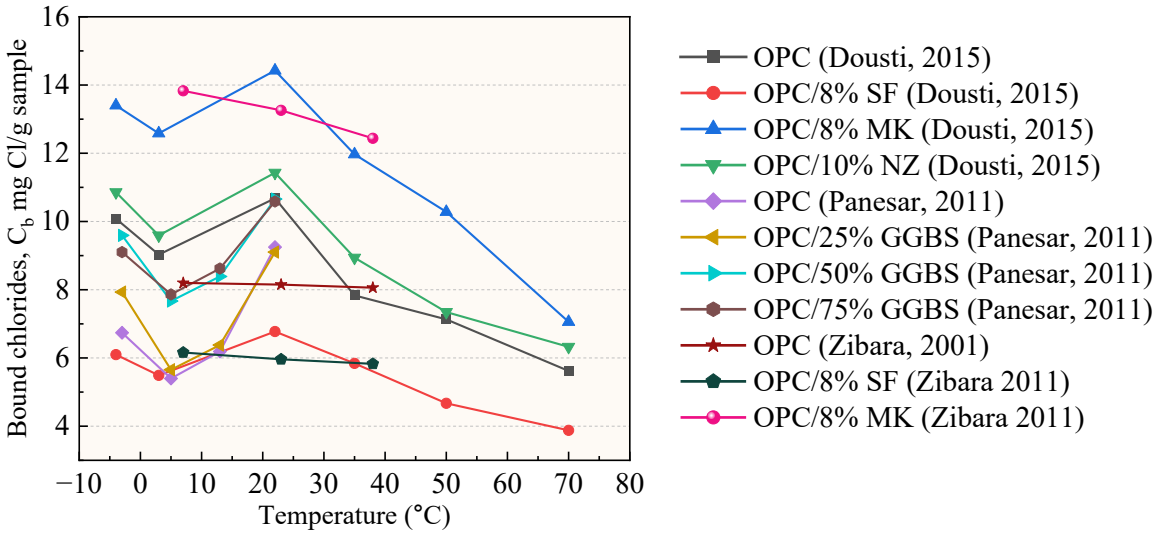

Fig. 3. Bound chloride contents in equilibrium with 1M free chloride concentration at different temperatures (data obtained from (Dousti and Shekarchi, 2015); (Panesar and Chidiac, 2011); (Zibara, 2001))

Effect on chloride ion transport rate

In addition to affecting the chloride binding ability of concrete, the surrounding temperature also influences the mobility of chloride ions through the pores in concrete. Studies investigating the temperature effect on chloride transport have used constant temperature (Care, 2008; Dousti et al., 2013; Yuan et al., 2008) or temperature gradient (Isteita and Xi, 2017) under natural diffusion and electric migration tests. All the investigations observed a higher chloride permeability and higher penetration depth with temperature rise. The primary reason attributed for the increased permeability was increased porosity and macroscopic crack network formed in concrete after exposure to even temperatures as low as 45˚C (Care, 2008). The chloride permeability is usually measured in terms of diffusion coefficients and can be measured using the Arrhenius equation to account for different temperatures (Equation 2).

$$D_2 = D_1 e^{\frac{E_a}{R}\left(\frac{1}{T_1}-\frac{1}{T_2}\right)} \quad (2)$$

Where D_1 and D_2 represent the diffusion coefficients at temperatures T_1 and T_2, respectively; E_a is the activation energy for chloride transport in the concrete, and R is the gas constant. Thus, increased activation energy results in greater susceptibility of concrete to chloride permeability at higher temperatures. The activation energies of different concrete mixes have been provided in Fig. 4. The detailed experimental methodology is provided in Table 3 of the Appendix. It can be observed that the activation energy of concretes with the same mix proportions also varies with the exposure duration, e.g., with longer immersion periods, the activation energy increases. Additionally, it can also be observed that for concretes using different water/binder ratios, the activation energy changes significantly once the water-to-binder ratio exceeds 0.5 due to the availability of largely unconstrained capillaries (Yuan et al., 2008). This is a cause for greater temperature susceptibility of concrete with high water-to-binder ratios (Page et al., 1981; Yuan et al., 2008). In some cases, high-temperature exposure has also been reported to increase the surface chloride concentrations in concretes (Samson and Marchand, 2007).

However, the adverse effect of temperature on chloride permeability has been observed to reduce in concretes containing different supplementary cementitious materials (SCMs). One of the reasons for this effect is the decreased activation energy of concrete with the addition of SCMs (Dousti et al., 2013; Nguyen et al., 2009). Dhir (Dhir et al., 1993) pointed out that high-temperature exposure also leads to a greater pozzolanic effect of SCMs such as fly ash (FA) and results in concrete densification, compensating for increased ionic diffusion. However, this beneficial effect of FA was prominent for higher cement replacement by FA in the mixing concrete.

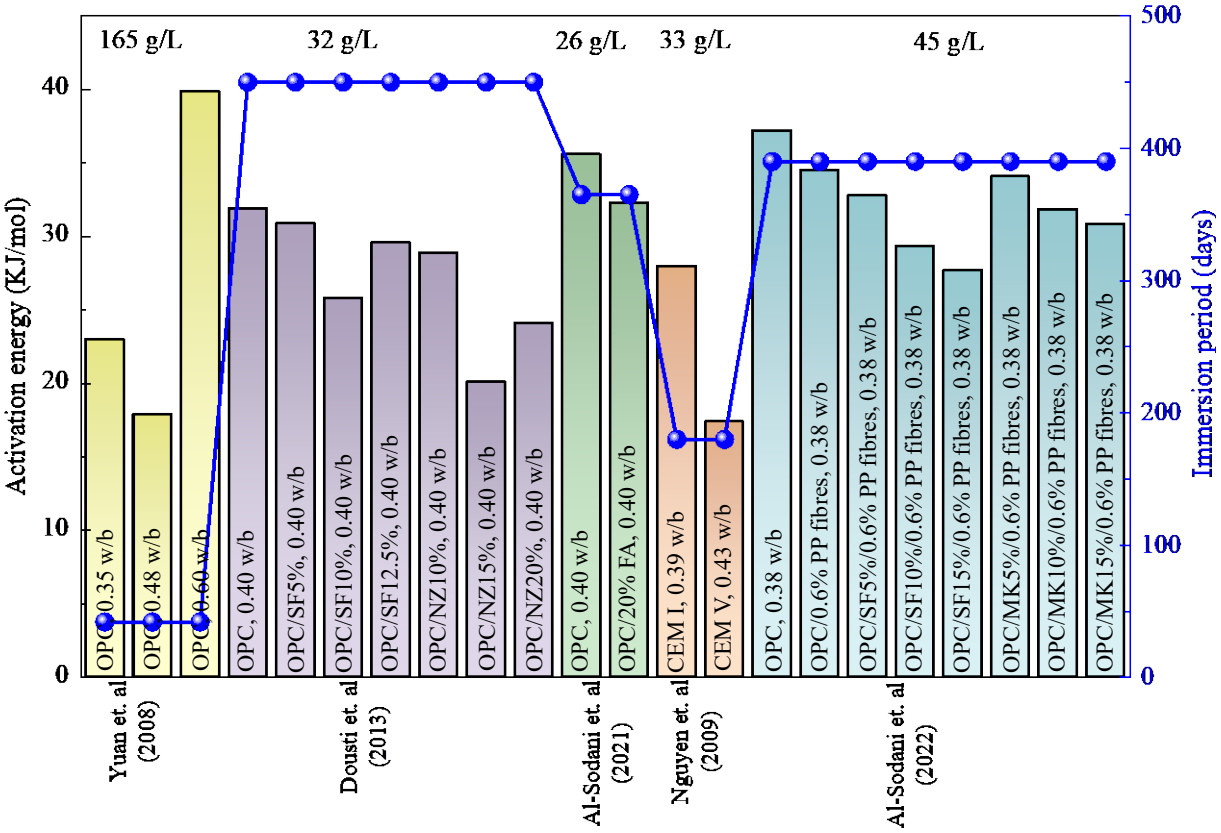

Fig. 4. Activation energy of concrete mixes obtained from the diffusion coefficient of chlorides of concretes at different temperatures when immersed in chloride solutions (data obtained from (Al-Sodani, 2022; Al-Sodani et al., 2021; Dousti et al., 2013; Nguyen et al., 2009; Yuan et al., 2008))*

**SF (Silica fume), NZ (Natural zeolite), FA (fly ash), MK (Metakaolin), PP(Polypropylene fibres), OPC(ordinary Portland cement), w/b (water to binder ratio)*

3.5 Effect of carbon dioxide ingress

Carbon dioxide (CO_2) from the atmosphere slowly diffuses into porous concrete during its service life and reacts with concrete's alkaline constituents in a moist environment. This reaction is called carbonation and leads to a drop in the alkalinity of the pore solution. This drop in pH results in the release of chloride ions bound to the different hydration products, thereby increasing the concentration of free chlorides (i.e., increasing the corrosion risk). In addition to releasing the bound chlorides, the interaction between CO_2 and cement hydration products also changes the concrete pore structure.

However, it has been identified that both these effects (i.e., the release of bound chlorides and changes in concrete pore structure) are dependent on the extent of carbonation and the nature of cement hydration products (von Greve-Dierfeld et al., 2020).

Attempts to study the synergistic effects of carbonation on chloride transport properties have generally employed two experimental sequences:

a) Carbonation followed by chloride attack

b) Chloride attack followed by carbonation

Carbonation followed by chloride exposure

This scenario represents the chloride transport process through the carbonated top surface layer of the concrete cover of RC structures. The progress of the carbonation front induces changes in pore structure (Ngala and Page, 1997) and near-surface microcracking (Wang et al., 2017). This significantly changes the chloride diffusivity in all the concrete types. A detailed figure highlighting the effect of carbonation on chloride diffusion rate, as observed in previous literature studies, is presented in Fig. 5. The detailed experimental conditions are listed in Table 4 of the Appendix. It can be observed that there is a wide variation concerning the influence of carbonation on chloride diffusion coefficient brought about broadly by the difference in concrete properties and carbonation exposure scheme (Holthuizen et al., 2018; Jin et al., 2018; Li et al., 2018; Liu et al., 2016b; Liu et al., 2017a; Malheiro et al., 2020; Wang et al., 2017; Xie et al., 2019)).

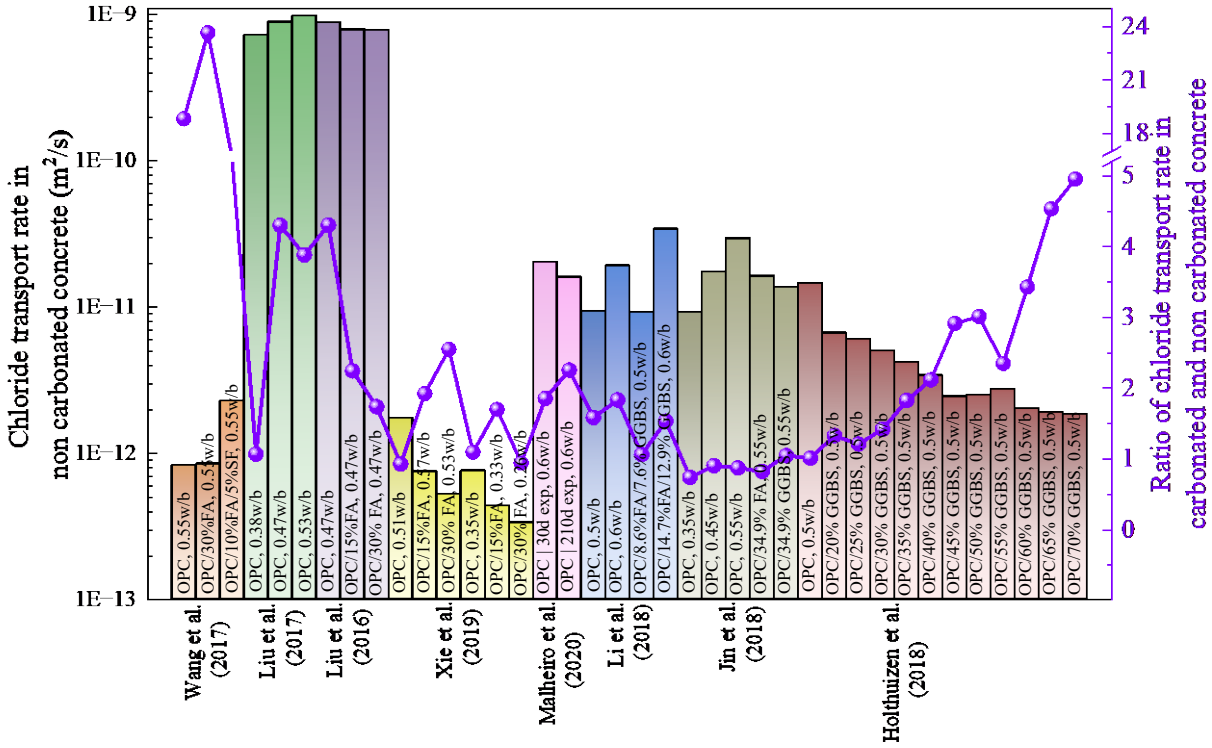

330

331 **Fig. 5.** Effect of prior carbonation on chloride diffusion coefficients through different concrete mixes
332 (data obtained from (Holthuizen et al., 2018; Jin et al., 2018; Li et al., 2018; Liu et al., 2016b; Liu et
333 al., 2017a; Malheiro et al., 2020; Wang et al., 2017; Xie et al., 2019)).

334 Once CO_2 penetrates the concrete, it reacts with different hydration products such as calcium hydroxide
335 (CH) and calcium silicate hydrate (CSH) and unhydrated constituents (C_3S and C_2S). CH most readily
336 reacts with CO_2 to form calcium carbonate among the different cement hydrates. The volume of calcium
337 carbonate formed by carbonation of CH is higher than the reactant and decreases concrete porosity.
338 After destabilizing all the accessible CH, calcium silicate hydrate (CSH) carbonation starts,
339 accompanied by several other hydrates. The carbonation of CSH involves a complex decalcification –
340 polymerization reaction with the formation of silica gel and the release of some water. Studies have
341 pointed out that the properties of CSH (i.e., Ca/Si ratio and water content) determine whether its
342 carbonation will have a net positive or negative volume change. For Portland cement pastes, the CSH
343 gel generally comprises a Ca/Si ratio between 1.5 and 1.9 with a jennite-like structure (Lothenbach et
344 al., 2011). However, adding silica-rich SCMs as a partial replacement for OPC leads to the formation
345 of tobermorite-like structured CSH gels with a lower Ca/Si ratio and more defects. It has been observed

346 that the most significant shrinkage due to carbonation happens in these lower Ca/Si characterized CSH
347 hydrates (Ca/Si less than 1.2) which increase the porosity of the concerned paste after carbonation (Chen
348 et al., 2006; Justnes et al., 2020; von Greve-Dierfeld et al., 2020). The replacement levels of SCMs
349 which trigger this transition vary significantly with the CaO content of the SCMs and can be identified
350 using thermodynamic modelling (Lothenbach et al., 2011). It has been observed that the transition of
351 CSH from a high Ca/Si ratio to a low Ca/Si generally takes place with the addition of about 15% SF or
352 20% FA, or 65% GGBS. However, this transition threshold changes with concrete's age and
353 composition due to the variations in anhydrous and hydrated phase contents (Saillio et al., 2019). Thus,
354 the CaO content of SCMs and the mixing amount significantly affect the chloride diffusion behaviour
355 of concrete after carbonation (Saillio et al., 2021; von Greve-Dierfeld et al., 2020).

356 Studies on the effect of GGBS have reported a fairly consistent trend with higher GGBS replacement
357 leading to a higher diffusion ratio (ratio of chloride rate in carbonated and non-carbonated concrete) in
358 all cases and is attributed to the increased carbonation depth (Holthuizen et al., 2018; Jin et al., 2018).
359 However, studies investigating FA-modified concrete have reported contrasting results. Xie et al. (Xie
360 et al., 2019) observed that when cement was replaced up to 30% by weight of FA, there was always an
361 increase in diffusion ratio, with a lower diffusion ratio observed in concretes prepared with a lower
362 water to binder (w/b) ratio. However, Liu et al. (Liu et al., 2016b) and Jin et al. (Jin et al., 2018) observed
363 a decrease in diffusion ratio on increasing FA content, aligning with the pore structure analysis by Wu
364 and Ye (Wu and Ye, 2017).

365 An increased water/binder ratio in OPC has been attributed to increasing cement hydration, increasing
366 the available CaO for reaction with CO_2 (Jin et al., 2018; Xie et al., 2019) and the subsequent
367 densification (i.e., decreased porosity). This can lead to a more remarkable decrease in the chloride
368 diffusion coefficient of OPC concretes after carbonation. However, these results have been contradicted
369 by observations from Liu et al. (Liu et al., 2017a) and Wang et al. (Wang et al., 2017), where the chloride
370 diffusion coefficient increased after carbonation when the w/b ratio employed was 0.47 or higher. Wang
371 et al. (Wang et al., 2017) attributed this to the development of shrinkage cracks in CSH when subjected
372 to accelerated carbonation.

In addition to concrete mix properties, the nature of CO_2 exposure scheme also affects its chloride diffusivity. Increased exposure to CO_2 increases the amount of CO_2 that can react with the hydration products and feature a deeper penetration into the concrete. This may amplify the effect of carbonation on chloride diffusion coefficient, as observed previously (Malheiro et al., 2020). However, it has been observed that the extent of interaction decreases with the exposure time, with the most significant decalcification of cement hydrates taking place in the first month of exposure to CO_2 (Wang et al., 2017).

In addition to modifying the chloride diffusivity, the new products formed by the carbonation process reduce the ability of the matrix to bind chlorides. Generally, for chloride ingress from an external source, the chlorides can bind physically to CSH gels due to their large surface area or get chemically bound to form Friedel's salt through its reaction with aluminate-ferrite-monosubstituted phases (AFm). This chloride binding ability greatly depends on the alumina content of the binder. Hence, the chloride binding increases with the addition of SCMs like metakaolin, GGBS and FA but decreases with SF (Thomas et al., 2012). In the case of carbonation, these AFm phases react with carbonate ions to form monocarboaluminate (Mc) phases, thus reducing the availability of AFm to bind the incoming chlorides chemically (Balonis et al., 2010; Chang, 2017). It is worth noting that some previous research works have shown that in the presence of high chloride ions, the carbonate ions can be replaced by chloride ions to form Friedel's salt. However, the extent of this reaction is minimal. Thus, the ability of carbonated binders to bind ingressed chlorides at a later stage is very low (Saillio et al., 2014).

Chloride exposure followed by carbonation:

This scenario represents the progress of carbonation front into the inner layers of concrete cover of RC structure. Since carbonation is a slow process that may take years to progress, it can be assumed that a considerable amount of chlorides might have already been ingressed into the structure and are bound to the hydration products. A schematic diagram demonstrating the effect of carbonation on chloride-contaminated concrete has been provided in Fig. 6. The main consequence of carbonation in concretes containing chlorides is a decrease in the pH of the pore solution and subsequent release of chlorides bound to the hydration products. Geng et al. (Geng et al., 2016) found that the release of chlorides is

400 facilitated by the decomposition of both CSH and Friedel salt, which are responsible for the physical
401 and chemical chloride binding, respectively.

402 In experiments that investigated the effect of carbonation on chloride-contaminated concrete, there was
403 significant chloride redistribution with deeper chloride penetration, a decrease in surface chloride
404 content and a slight inward shift in peak chloride front (Chang et al., 2018; Dousti and Khaksar, 2023;
405 Geng et al., 2016; Wang et al., 2017; Ye et al., 2016). A few reasons that were pointed out for this
406 phenomenon are (1) diffusion of free chlorides because of the concentration gradient; (2) maintaining
407 a charge balance after a decrease in OH^-; (3) subsequent inward movement of water generated through
408 carbonation carrying free chlorides. Further, it was observed that chloride contamination also reduced
409 the carbonation depth compared to regular concrete due to pore refinement (Kuosa et al., 2014; Liu et
410 al., 2017a). This was linked to the higher moisture content in the pores due to the hygroscopic nature
411 of chloride salts (Malheiro et al., 2021). When evaluating this effect on concretes with different
412 water/binder ratios, it was observed that the reduced carbonation front in chloride-contaminated
413 concrete was more prominent in concretes with lower water/binder ratios. In addition to high moisture
414 content, another reason pointed out was the ability of chlorides to block some of the concrete pores and
415 thus reduce CO_2 penetration (Li et al., 2024).

416 While carbonation has been observed to have a generally detrimental effect on chloride binding, one
417 study by Zheng et al. (Zheng et al., 2021) found that at low w/b ratios, mild carbonation led to increased
418 chloride binding. The hypothesis was that the carbonate deposits formed as a result of the reaction
419 blocked some of the concrete pores, trapping the free and adsorbed chlorides and inhibiting their
420 mobility.

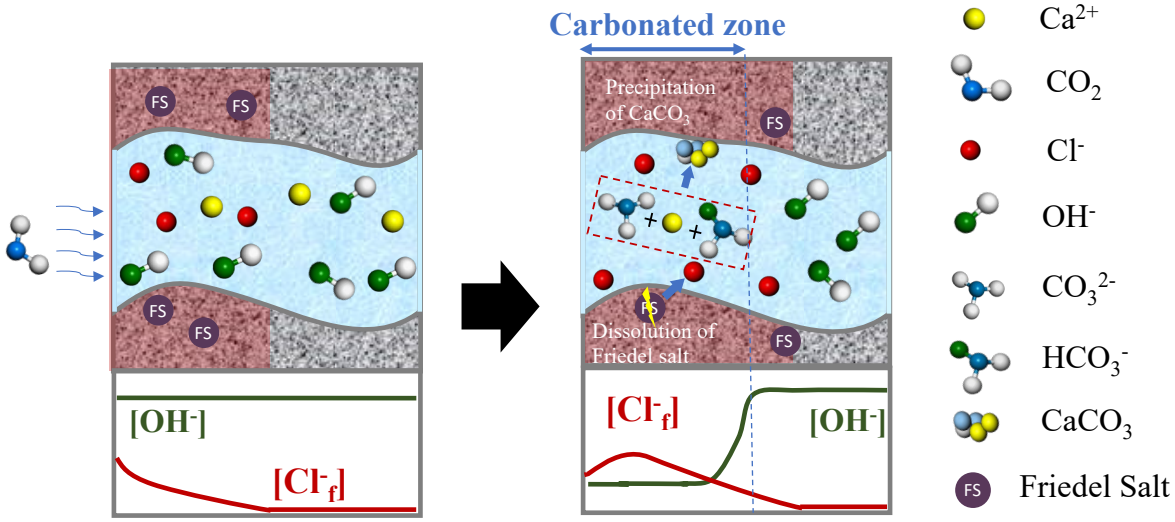

Fig. 6. Schematic of the effect of carbonation on chloride-contaminated concrete showing (i) reduction of OH^- concentration in the carbonated zone, (ii) decomposition of Friedel salt which increases the free chloride concentration, (iii) deeper penetration of free chlorides and shift of peak chloride concentration inside and (iv) reaction between carbonate ions or bicarbonate ions (produced from dissolution of CO_2) with calcium hydroxide to form calcium carbonate which precipitates in concrete pores

4. Effect of micro-climatic factors on chloride threshold

4.1. Effect of carbon dioxide ingress

A thin iron oxide film (passive film) is formed in an alkaline solution because of the reaction between metal and hydroxyl ions (Guzman et al., 1979). This phenomenon is called passivation, and the passive film grows to a steady thickness in nearly two weeks after casting (Poursaee and Hansson, 2007). As the chloride front goes inside concrete, it leads to leaching of alkalis. This progressively increases the $[Cl^-]/[OH^-]$ at steel surface and, with sufficient oxygen availability, leads to depassivation and an active corrosion state of the reinforcement (Melchers, 2020; Melchers and Chaves, 2020). Hence, the initial concentration of hydroxyl ions (i.e., pH of the solution) significantly affects steel's passivation and chloride threshold value. The influence of pH on the Tafel polarization plots has been extensively studied by Liu et al. (Liu et al., 2021) and validated using Mixed Potential Model (MPM). For a

deaerated solution, an increase in pH reduces the water reduction rate (responsible for cathodic half-cell reaction), leading to a lower current density. An increase in pH (pH > 12.5) also decreases the time required for steel passivation (Li et al., 2017) and affects the final steady potential. In addition to affecting the passive film properties and its protectiveness, even a minor decrease in pH reduces the chloride threshold value (Liu et al., 2016d; Liu et al., 2014). This highlights the importance of pH on corrosion initiation.

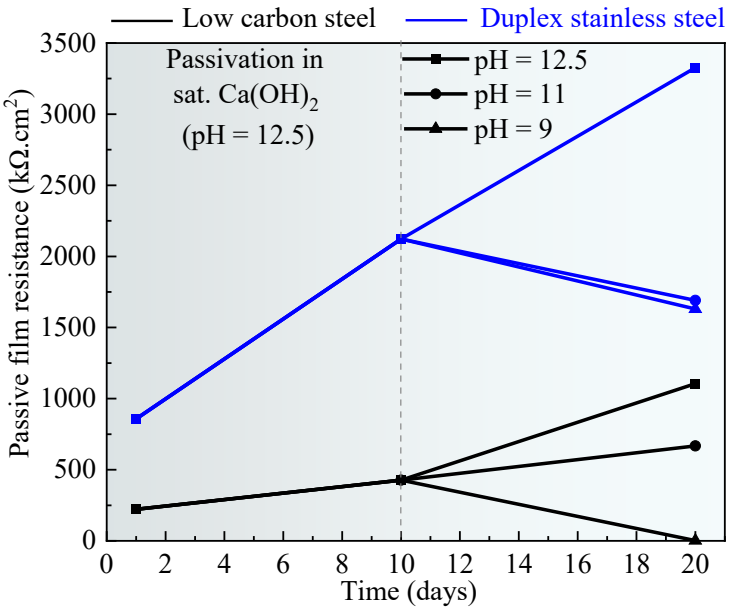

(a)

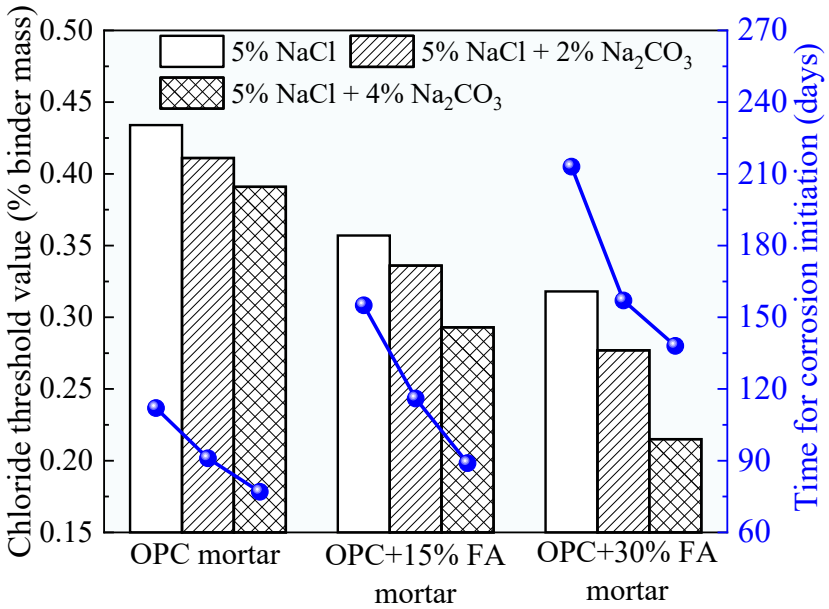

(b)

Fig. 7. Degradation effect due to carbonation on (a) passive film formed on steel in simulated pore solution (data obtained from Liu et al., 2016c) and (b) corrosion initiation time in mortars (data obtained from Shi et al., 2020)

Generally, the pH of the concrete's pore solution can vary significantly with the diffusion of CO_2. Several studies have added different concentrations of bicarbonate/carbonate ions to the pore solution to simulate the above situation (Liu et al., 2016d; Shi et al., 2020). In all the studies, it has been reported that the introduction of carbonate ions leads to a drop in passive film resistance (refer to Fig 7 (a)) such that, in very low pH systems (pH ~9), the steel corrosion can initiate even without chloride ions (Huet et al., 2005; Shi et al., 2020). Additionally, in such cases, it has been observed that passivation is relatively slower in the alkaline solution, along with a higher passive current density, denoting a porous passive film formation. The risk of pitting corrosion is also higher (Figueira et al., 2017; Liu et al., 2017b). However, the effect is highly dependent on the steel type. The sharp drop in pH of the concrete pore solution at severe carbonation changes the $[Cl^-]/[OH^-]$ significantly in the pore solution, increasing the corrosion susceptibility against chloride ions (De Weerdt et al., 2019; Hay and Celik, 2024; Liu et al., 2016d). This can be observed in Fig. 7 (b), with two different fly ash contents under combined chloride and carbonate ion penetration. With the addition of fly ash, the drop in chloride threshold value is more drastic, which aligns with the observations in Section 3. In fact, for severely carbonated concretes, adding fly ash has negligible benefit in delaying corrosion initiation time. Thus, based on the observations, the effect of pH and chloride ions on the anodic polarization curves of steel reinforcement can be represented as shown in Fig. 8 (Wang et al., 2016).

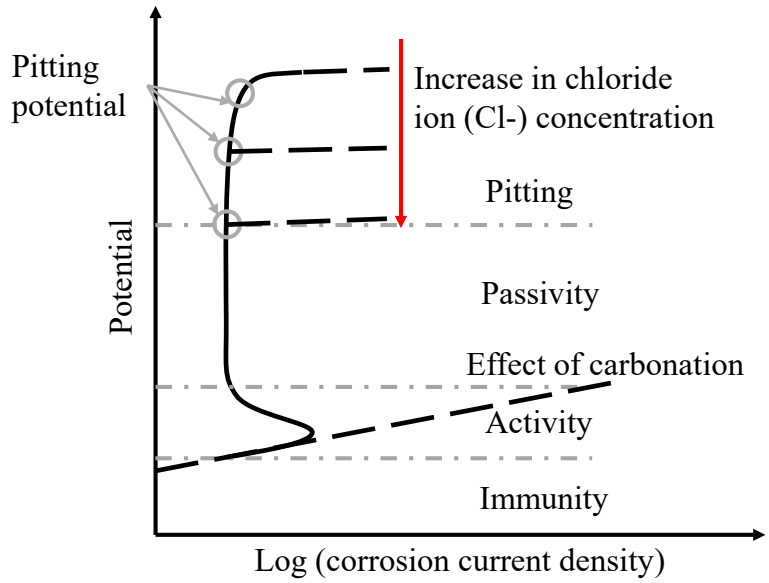

Fig. 8. Schematic diagram for anodic polarization curves under the effect of chloride ingress and carbonation showing (i) reduction of pitting potential with increasing chloride concentrations in concrete pore solution and (ii) breakdown of passivity and transformation of steel from passive to active state due to carbonation (Bertolini et al., 2013).

The ingress of carbon dioxide into concrete and the subsequent carbonation reactions also alter the pore structure, as explained in Section 3.5. This affects concrete resistance, primarily facilitating electron transfer between the anode and cathode. While this effect is negligible in microcell corrosion, the effect is significant for macrocell corrosion where the cathode and anodic regions are separated. The number of studies on this aspect is very limited. Revert et al. (Revert et al., 2019) investigated the effect of carbonation on macrocell corrosion current density for OPC and concretes with cement replacements of 18% and 30% by FA. They observed that the concrete resistance increased with fly ash addition for non-carbonated cases. When carbonated, the concretes with fly ash showed similar bulk resistance to OPC and a higher macrocell corrosion current density. Chen and Su (Chen and Su, 2023) extended this study to consider other SCMs like GGBS and SF. They observed increased macrocell current density irrespective of any SCM additions, suggesting that macrocell corrosion risk is highly intensified in SCM-modified concrete due to carbonation.

4.2. Effect of relative humidity and periodic wetting and drying

The moisture changes in concrete brought about by relative humidity in the atmosphere and periodic drying and wetting have two impacts: one is electrolytic resistance, responsible for electron transfer between anodic and cathodic sites, and the other is cathodic polarization resistance, which controls oxygen reduction at cathodic sites. When the concrete is completely dry, corrosion is inhibited due to the absence of any electrolyte for microcell and macrocell corrosion. When the concrete is fully submerged in water such that oxygen diffusion is restricted, the high cathodic polarization resistance is the controlling factor (Liu and Weyers, 1998).

For RC structures or some of its parts exposed to the atmosphere and well aerated, the internal humidity of concrete (i.e., moisture content) varies with the relative humidity of the atmosphere. A 12-month exposure study observed that the fluctuations in concrete internal humidity were less than atmospheric humidity, with the fluctuations being more significant in summer than in winter, suggesting that the temperature also plays an important role (Lu et al., 2017). Even the concrete composition seemed to affect the magnitude of changes in internal humidity. For example, the change was more significant for concretes with more than 30% FA contents and was attributed to the larger pores, allowing easier moisture exchange. It has been observed that the presence of chlorides in concrete can also increase the moisture content in concrete due to their hygroscopic effect (Bai et al., 2021). This is because the NaCl crystals get easily electrolysed to Na+ and Cl-, which react with water and increase porous concrete's overall moisture absorption capacity. This effect is pronounced in concretes with high chloride contents and at higher atmospheric relative humidity, which could increase the time of wetness of steel reinforcement and, thus, prolonged periods of high corrosion currents.

For RC structures in tidal and splash zones, periodic wetting and drying cycles are the influential factors changing the moisture state in concrete. Investigations relating corrosion current with the changes in concrete moisture state explained that the net corrosion current in the cathodic branch during wetting is due to the combination of two contrasting effects: an increase in current due to lowered electrolytic resistance and a decrease in current due to increased oxygen reduction resistance (Raupach, 1996a, b) (Andrade et al., 1990). Raupach (Raupach, 1996b) observed that electrolyte resistance played a dominating role in the short wetting phase of concrete. The corrosion current increased with moisture

uptake by concrete and gradually decreased after the concrete started drying as the electrolyte resistance increased. Oxygen availability plays a dominating role in the longer wetting phase of concrete. From its dry state, the current increased with moisture intake to reach a maximum, followed by a swift drop as the oxygen supply was limited. During the drying stage, a comparison of the corrosion current from two concretes with w/b ratios of 0.4 and 0.65 revealed that for high-resistivity concrete (0.4 w/b in this case), the corrosion current was controlled by concrete resistance (Otieno et al., 2019). In comparison, the corrosion current varied with electrolyte and cathodic resistance for low-resistivity concrete of 0.65 w/b. Stefanoni extended this study to multiple wetting and drying cycles and observed that the peak current achieved in the wetting stage decreased with subsequent cyclic exposure (Stefanoni et al., 2020). A schematic of the relationship between corrosion current and different water saturation levels is provided in Fig 9.

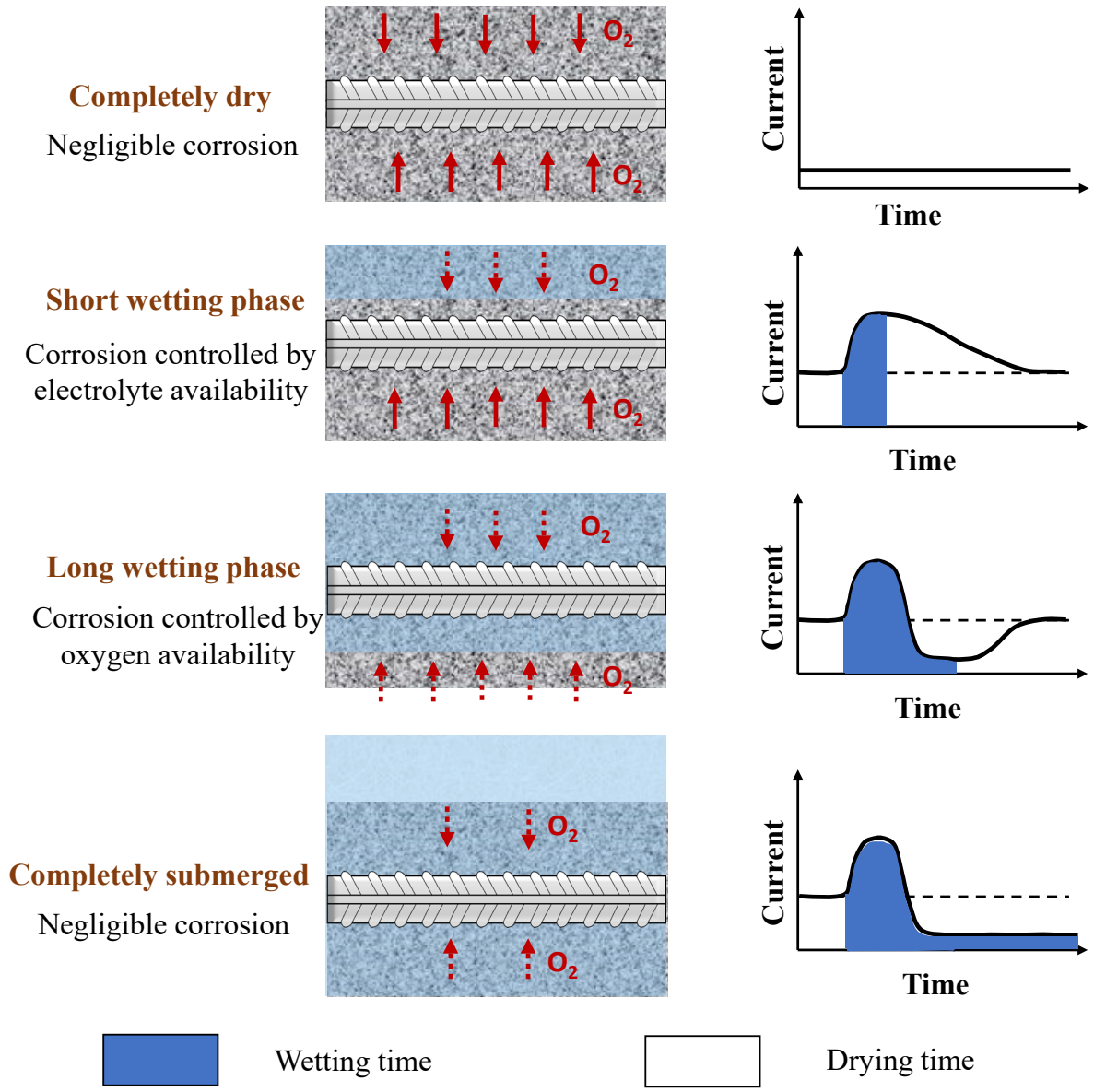

526

527 **Fig. 9.** Schematic diagram for the accessibility of oxygen to the steel surface when reinforced
528 concrete is subjected to four cases of exposure in periodic wetting and drying cycles of salt water and
529 the corresponding changes in corrosion current density controlled by electrolyte resistance and
530 oxygen reduction resistance (Raupach, 1996b)

531 The moisture content in the concrete pores influences the transport rate of oxygen. The available oxygen
532 at the steel surface influences the steel passivation behavior even without chlorides. Alhozaimy et al.
533 (Alhozaimy et al., 2016) observed that the initial current was low during passivation for reinforcing
534 steel in concrete cured in a sealed condition or submerged in water with minimal oxygen. However,
535 these steel specimens showed high corrosion rates in long-term exposure. This was attributed to the

poor passivation of steel reinforcement in the initial periods, thus making the steel vulnerable to corrosion. Decreasing the available oxygen decreases the cathodic current density and subsequently shifts the corrosion potential towards more negative values (Fig. 10). The relation between oxygen availability and corrosion potential is also strongly observed in the pore solution of binders containing GGBS, where an oxygen deficiency shifts the corrosion potential to even values of -1V vs SCE in some cases (Criado and Provis, 2018; Das et al., 2023; Mundra and Provis, 2021). Some studies have reported that such a negative potential shift due to oxygen unavailability also helps to inhibit any corrosion risk (as the case for steel immersed in seawater) (Hussain and Ishida, 2010).

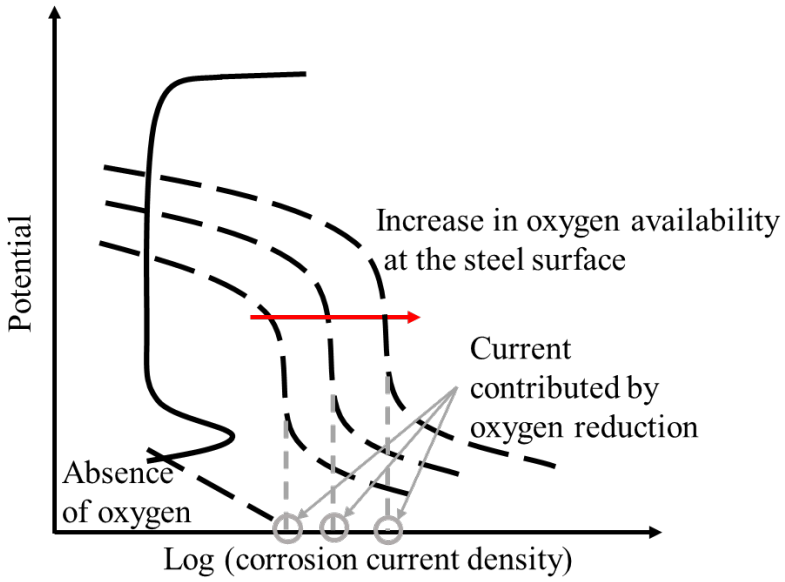

Fig. 10. Schematic diagram for cathodic polarization curves, which shows (i) increasing corrosion current density due to greater availability of oxygen at steel surface and (ii) negligible electrochemical reaction in the absence of oxygen (Bertolini et al., 2013)

While this observation was based on microcell current, it can also be extended to macrocell corrosion. Macrocell corrosion currents between actively corroding and passivated steel rebars are negligible in dry concrete due to high electrolytic resistivity. However, moisture ingress reduces resistivity, enabling significant galvanic currents. In partially submerged structures, submerged rebars (anodes) corrode aggressively, while aerated rebars (cathodes) sustain cathodic reactions, as demonstrated before (Chalhoub et al., 2020; Li et al., 2023a). The time for corrosion initiation depends critically on the

cathode-to-anode (C/A) area ratio. Li et al. (Li et al., 2023b) reported that increasing the C/A ratio from 1 to 2 reduced the chloride threshold required for active corrosion by up to 50%, attributing this to intensified Cl^- adsorption at anodic sites. This adsorption promoted cation vacancy formation in the passive film, destabilizing its protective oxide layer and accelerating localized pitting. As a result, the corrosion initiation time was shortened.

4.3. Effect of temperature

A reinforced structure is constantly subjected to temperature fluctuations, which affect the corrosion rate. Jiang and Yuan (Jiang and Yuan, 2013) evaluated the variation of concrete's internal temperature based on natural climate and found that the variations in concrete's internal temperature followed the same trend as external climate. However, a difference of 1 to 2°F could be observed at the location of steel reinforcement when there are significant changes in concrete cover thickness (Liu and Weyers, 1998). Thus, many studies have been carried out by using concrete's pore solution of different temperatures to simulate different climatic conditions. When the environment temperature is increased, keeping both the pH and dissolved oxygen (DO) constant, it has been observed that the changes in the curves follow the Arrhenius behavior leading to increased corrosion current density (Liu et al., 2021). The exposure temperature also affects the passive film growth rate and composition. It has been observed that an increase in temperature reduces the Fe (II)/ Fe (III) ratio as well as the ratio of Fe (oxides)/ Fe (hydroxides) in the developed passive film over carbon steel in an alkaline solution (Deus et al., 2012). These differences in passive film composition are attributed as one of the reasons for the negative shift in potential with high temperatures (Abd El Haleem et al., 2010; Sánchez-Moreno et al., 2009). An increased temperature has also been observed to alter the semiconductor properties of the formed passive film, which increases the passive current density (Wang et al., 2021). In addition to affecting the passive film properties, the exposure of steel rebars to higher temperatures causes a negative shift in the breakdown potential and decreases its localized corrosion resistance to chloride ions (Sharifi-Asl et al., 2015; Zha et al., 2022). However, the influence of temperature on corrosion risk does not feature a constant value and varies with the type of steel reinforcement (i.e., alloy composition). In a study comprising different stainless steels, it was observed that the low nickel duplex steels, due to

their low nickel and high manganese content, exhibited higher sensitivity to temperature over austenitic steels (Gastaldi and Bertolini, 2014). This led to the pitting corrosion initiation of low nickel duplex steels at a much lower chloride content of 2.5% by mass of cement at 40˚C compared to 3% at 20˚C.

While most experimental studies involve exposure to a constant temperature, the temperature fluctuates with varying frequency and amplitude in real scenarios. A study by Feng et al. (Feng et al., 2020) observed that high frequency and high amplitude of temperature variations led to localized breakdown and cracks in the passive film due to the varying thermal expansion coefficients of steel and passive film. The temperature cycles also induce mechanical stresses at the steel-concrete interface due to the subsequent changes in the volume of oxide layers, leading to durability issues (Díaz et al., 2018). In addition to the prevailing temperature, some studies (Poursaee, 2016; Ruan et al., 2015) have observed that the previous exposure history of steel to high temperatures (such as in fire) can reduce the protectiveness of passive film formed on the steel surface when immersed in an alkaline solution. This developed passive film has also been observed to be sensitive to the use of different methods, such as air or water, to cool down the steel reinforcements, which can incur significant changes in the microstructure of steel specimens. The steel samples cooled with the use of water post-fire exposure show an increase in the amount of martensite phase, which is primarily responsible for their poor passivation.

Some commonly occurring situations that can expose steel reinforcements to high temperatures are the different curing regimes or extreme environmental conditions. It has been observed that during concrete casting, high-temperature in rebars can increase the porosity at the steel/concrete interface (SCI), leading to lower bond strength (Pati, 2010). Subsequently, the porous SCI increases the corrosion susceptibility of the steel reinforcement in these members (Chen and Su, 2020).

However, it has been observed that the sensitivity of steel reinforcement to temperature changes decreases with an increase in the concrete resistivity (i.e., high-quality concrete) and increasing cover depth for reinforced concrete. Pour-Ghaz et al. (Pour-Ghaz et al., 2009a, b) observed from experimental studies and numerical modelling that the corrosion process was controlled by the resistivity of concrete

607 for high-quality concrete. Therefore, corrosion kinetics' dependence on such concrete's temperature was
608 limited.

609 5. Discussion and future perspectives

610 Based on the review, a detailed illustration of the role of micro-climate parameters on the corrosion
611 initiation process is provided in Fig. 11, following equations by (Li and Song, 2022; Meira et al., 2008;
612 Pour-Ghaz et al., 2009a).

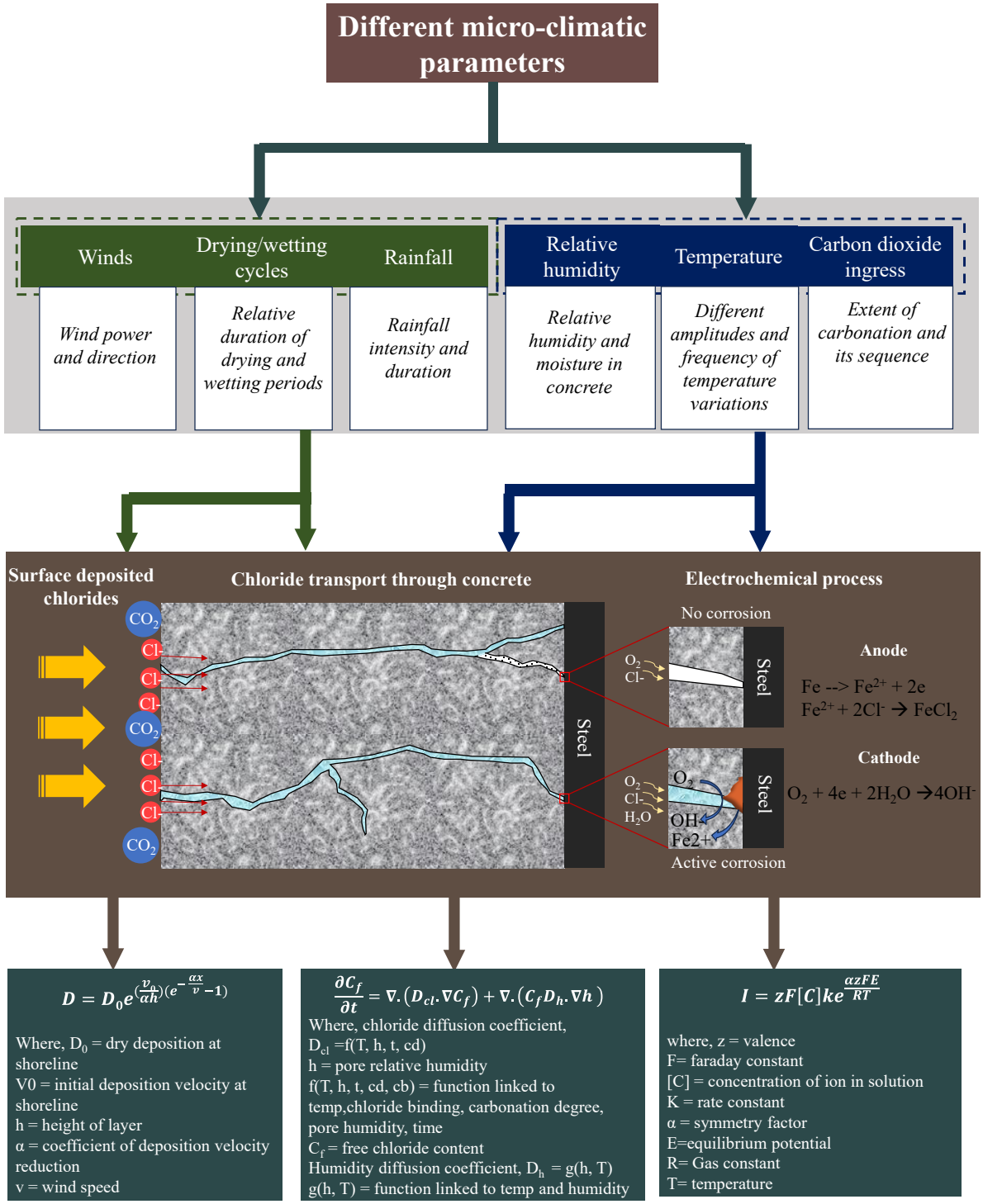

Fig. 11. Schematic diagram showing the main micro-climate factors that affect (i) the nature and transport rate of chlorides through concrete and (ii) chloride threshold value required for steel corrosion initiation

5.1 Chloride transport

Studies aimed to address micro-climates' effects have employed wet-dry cyclical exposure schemes or, in some cases, subjected them to field exposures. However, there are some main challenges associated with evaluating their effect:

i) Very limited studies have been conducted to specifically evaluate the changes in convection depth and peak chloride contents with wet/dry cycles for different concrete mixes. The role of SCMs is controversial regarding their use in concretes exposed to wet-dry cycles, considering contradictory results in the literature.

ii) There is inconsistency in the number of wetting and drying periods hours in different studies, which makes comparing different parameters difficult.

iii) The effect of rainfall and wind on chloride transport characteristics in concrete (i.e., chloride transport rate and chloride binding properties) is still relatively unexplored.

Even for the same mechanism of chloride transport through concrete, the exposure temperature changes the chloride transport rate (Al-Sodani, 2022; Yuan et al., 2008). This increase is considered to be governed by the activation energy of the concrete mix, which is obtained from diffusion experiments. There are three main concerns with the conducted studies:

i) The studies have calculated activation energy based on the chloride transport rate observed through diffusion experiments. These studies have been conducted at different concrete ages and for different chloride exposure conditions. Thus, the activation energy from different studies differs even for the same concrete mix.

ii) It is unclear how the activation energy changes when chloride transport is conducted under accelerated conditions (i.e., applied voltage).

iii) The inconsistency between the age of concrete when evaluating chloride binding ability at different temperatures among the available studies makes their comparison difficult. There

642 also seems to be no consensus on the mechanism behind chloride binding at different
643 temperatures and the effect of concrete mix.

644 Considering the chloride transport through concrete pores, changes in pore distribution due to
645 carbonation also affect the resultant chloride transport. The observations from the literature suggest that
646 carbonation may have beneficial or detrimental effects on chloride transport rate based on concrete mix
647 proportions. Over the last few decades, there has been an increasing addition of SCMs in concrete and
648 the development of sustainable binder systems (LC3 and alkali-activated materials). Thus, it is
649 imperative to understand how these binders perform under combined carbonation and chloride
650 exposure. Additionally, volume change as a result of carbonation of CSH with different Ca/Si ranges
651 could be conducted to consider changes in porosity.

652 **5.2 Chloride threshold**

653 In the event of carbonation, where the pH of the concrete pore solution may drop to about 9, literature
654 studies reveal that corrosion may initiate even in the absence of chloride ions. Despite the available
655 literature, some aspects need more investigation:

656 i) Studies evaluating the risk of carbonation on steel corrosion have added various dosages of
657 carbonate and bicarbonate ions to simulated pore solutions, usually cement pore solutions or
658 saturated $Ca(OH)_2$. It is worth mentioning that during carbonation, there are changes in
659 concrete pore solution with the uptake of alkali metals by carbonated hydrates (De Weerdt et
660 al., 2019). This situation will not be reflected in the current setup, so the corrosion risk may be
661 over or underestimated. Thus, the reliability of results in simulated pore solutions should be
662 further explored. Additionally, the correlation between simulated carbonated pore solution and
663 real concrete environment needs to be revealed.

664 ii) Available studies have only emphasized plain cement mixes. With the development of
665 sustainable binders, which are more prone to carbonation, more studies are required to develop
666 the necessary understanding.

Since oxygen reduction is the primary cathodic reaction, the availability of oxygen affects both the passivation in an alkaline environment and depassivation in the presence of chlorides. There are two aspects relating to oxygen availability and corrosion risk that require further investigation:

i) Once the chlorides have sufficiently ingressed the concretes, they will affect the concrete's internal humidity (pore saturation), affecting the wetness time of reinforcement and corrosion current. Thus, the changes in corrosion current due to this mechanism need further investigation.

ii) Limited studies are available to understand the macrocell corrosion risk in undersea transport tunnels where one side of the structure is exposed to seawater and the other is aerated. Critical factors such as hydrostatic pressure, concrete mix and chloride ingress profile require systematic investigations to quantify their risk.

iii) It is relatively unclear whether a combination of the reducing chemical nature of binder and dense matrix, which can reduce oxygen access to the steel surface, may restrict corrosion even in the presence of chlorides.

Very limited studies have tried to understand the effect of the corrosion risk of steel in alkaline solutions at different temperatures and the underlying mechanism, especially the effect on passivation and depassivation mechanism. With the development of different strength grades and alloy composition of steel, their corrosion susceptibility at different temperatures remains to be investigated.

Distinct microclimates within structural elements establish electrochemical potential differences between adjacent steel regions, driving macrocell corrosion currents. As mentioned in previous sections, the severity of such corrosion depends on three key factors: (1) the chemical composition of the concrete (e.g., chloride content, pH), (2) the moisture content governing electrolytic conductivity, and (3) the cathode-to-anode (C/A) area ratio, which amplifies localized corrosion rates. Understanding this multi-faceted phenomenon—governed by coupled electrochemical, environmental, and material interactions—is essential for designing structures in harsh environments (e.g., marine, industrial).

692 Conventional durability design standards, including ACI, EN, GB, and AS, categorize marine exposure
693 environments into distinct severity classifications—such as fully submerged, tidal/splash, and airborne
694 chloride conditions—without addressing site-specific environmental variability (Hooton, 2019). The
695 FIB Model Code 2010 introduces a progressive shift by adopting probabilistic modeling to
696 accommodate data variability and forecast the probability of steel depassivation at defined chloride
697 thresholds. While existing probabilistic frameworks acknowledge uncertainties in micro-climatic
698 parameters (e.g., temperature gradients, CO_2 diffusion), their treatment of interactions between these
699 factors and corrosion kinetics remains overly simplistic (Bastidas-Arteaga et al., 2010; Stewart et al.,
700 2011). By establishing improved relationships between micro-climate parameters and electro-physical-
701 chemical aspects of the corrosion process, these insights can be incorporated into service life models to
702 refine stochastic variables and multi-physics coupling, thereby improving their accuracy. The prediction
703 models can be further enhanced when combined with climate projections, which capture daily and
704 seasonal variations and uncertainties associated with future climate in a location (Guo et al., 2020)
705 Successfully incorporating these understandings would advance probability-based durability standards
706 and ultimately enable the development of climate-resilient infrastructure in the long run.

707 # 6. Summary

708 Based on the literature review, the following conclusions are drawn:

709 1. The convection depth is formed in the top 15 mm layer of concrete due to rapid changes in pore
710 moisture content brought by atmospheric humidity, rainfall, wetting and drying cycles of salt water.
711 The convection depth and peak chloride content seem to be directly linked to the w/b ratio of the
712 mixes due to the presence of larger pores. However, the concrete mix composition has limited
713 effect. The convection depth increases with a greater drying/wetting period and an increasing
714 exposure period, resulting in increased chloride contents in concrete interiors.

715 2. The moisture state of concrete by micro-climatic factors influences the electrochemical reactions
716 by changing the electrolyte and cathodic polarization resistance. When the concrete's moisture
717 content increases from its original dry state during the wetting cycle, the reduced electrolyte

718 resistance leads to increased corrosion current. However, with the prolonged wetting stage, the
719 oxygen availability at the steel surface decreases, thereby reducing the corrosion current. When the
720 concrete is dry, the corrosion current is controlled by electrolyte resistance for high-resistivity
721 concrete and combined electrolytic and cathodic polarisation resistance for low-resistivity concrete.

722 3. For the carbonated layer of concrete, the rate of chloride transport is changed considerably by pore
723 redistribution and microcracking. The carbonation leads to a net reduction of porosity and chloride
724 transport rate for OPC concrete with a low w/b ratio. For high w/b ratio and concretes with silica-
725 rich SCMs (leading to low Ca/Si ratio based CSH gels), the carbonation causes the coarsening of
726 pores and reduces the time for chlorides to reach the steel surface. The carbonation front progression
727 into deeper chloride-contaminated concrete layers leads to the release of bound chlorides,
728 increasing free chloride amounts in the inner concrete layers.

729 4. In addition to releasing the bound chlorides, the progress of the carbonation front near the steel
730 surface in chloride-contaminated concrete reduces the pore solution pH, which sharply increases
731 [Cl]/[OH] steel surface. As a result, the corrosion initiation time is shortened significantly. Only in
732 those cases where the release of bound chlorides due to carbonation is compensated by reduced
733 chloride transport rate could a net increase in corrosion initiation time be observed.

734 5. The surrounding temperature directly impacts ionic mobility and the bound chloride contents,
735 ultimately influencing the chloride distribution inside the concrete. The increased chloride transport
736 rate can be explained by activation energy, which reduces with increasing SCM content in the
737 concrete mix. The bound chloride contents do not show a definitive trend but vary significantly
738 with exposed temperature.

739 6. Increased temperature leads to a porous and defective passive film on steel, which reduces the
740 chloride threshold for corrosion initiation. One reason for the localised defects is the different
741 thermal coefficients of expansion for steel and passive film. Increasing temperature also leads to a
742 negative shift in breakdown potential, which raises the localized corrosion risk.

7. Considering the significant role of micro-climates, a more realistic assessment of chloride-induced corrosion initiation time should include chloride transport rate and threshold values modified by seasonal and daily temperature trends, humidity for the atmospheric zone and accurate wetting and drying periods of structural members for tidal and splash exposure zones. The effect of carbonation should account for the chemistry of the binder such that the net impact on the chloride transport rate is accurately considered. These steps will ensure that the structure meets its design service periods without requiring extensive maintenance.

8. It is suggested that design engineers should improve their understanding of the influence of micro-climate factors on chloride-induced corrosion. This would enable them to choose the appropriate environmental loads when designing coastal RC structures, leading to efficient resource allocation.

Acknowledgments

The authors would like to thank Guangdong Province R&D Plan for Key Areas (Project code: 2019B111107002) and the Hong Kong Research Grants Council - Theme-based Research Scheme (Project code: T22-5-2/18-R) for the financial support of this research project. The second author acknowledges the support of National Natural Science Foundation of China (52308247). The authors thank Professor Robert Melchers of Newcastle University for his valuable suggestions and discussions.

References

Abd El Haleem, S., Abd El Aal, E., Abd El Wanees, S., Diab, A., 2010. Environmental factors affecting the corrosion behaviour of reinforcing steel: I. The early stage of passive film formation in Ca (OH) 2 solutions. Corrosion Science 52 (12), 3875-3882.

Al-Sodani, K.A.A., 2022. Effect of exposure temperatures on chloride penetration resistance of concrete incorporating polypropylene Fibers, silica fume and metakaolin. Construction and Building Materials 346, 128445.

768 Al-Sodani, K.A.A., Al-Zahrani, M.M., Maslehuddin, M., Al-Amoudi, O.S.B., Al-Dulaijan, S.U., 2021.
769 Chloride diffusion models for Type I and fly ash cement concrete exposed to field and laboratory
770 conditions. Marine Structures 76, 102900.
771 Alhozaimy, A., Hussain, R.R., Al-Negheimish, A., 2016. Significance of oxygen concentration on the
772 quality of passive film formation for steel reinforced concrete structures during the initial curing of
773 concrete. Cement and Concrete Composites 65, 171-176.
774 Ambler, H., Bain, A., 1955. Corrosion of metals in the tropics. Journal of Applied Chemistry 5 (9), 437-
775 467.
776 Andrade, C., Alonso, C., Garcia, A., 1990. Oxygen availability in the corrosion of reinforcements.
777 Advances in cement research 3 (11), 127-132.
778 Andrade, C., Alonso, C., Sarría, J., 2002. Corrosion rate evolution in concrete structures exposed to the
779 atmosphere. Cement and Concrete Composites 24 (1), 55-64.
780 Andrade, C., Sarría, J., Alonso, C., 1999. Relative humidity in the interior of concrete exposed to natural
781 and artificial weathering. Cement and Concrete Research 29 (8), 1249-1259.
782 Angst, U., Elsener, B., Larsen, C.K., Vennesland, Ø., 2009. Critical chloride content in reinforced
783 concrete—A review. Cement and Concrete Research 39 (12), 1122-1138.
784 Ann, K.Y., Song, H.-W., 2007. Chloride threshold level for corrosion of steel in concrete. Corrosion
785 Science 49 (11), 4113-4133.
786 Arya, C., Bioubakhsh, S., Vassie, P., 2014. Chloride penetration in concrete subject to wet/dry cycling:
787 influence of moisture content. Proceedings of the Institution of Civil Engineers-Structures and
788 Buildings 167 (2), 94-107.
789 Bai, L., Xie, J., Liu, J., Xie, Y., 2021. Effect of salt on hygroscopic properties of cement mortar.
790 Construction and Building Materials 305, 124746.
791 Balonis, M., Lothenbach, B., Le Saout, G., Glasser, F.P., 2010. Impact of chloride on the mineralogy of
792 hydrated Portland cement systems. Cement and Concrete Research 40 (7), 1009-1022.
793 Bastidas-Arteaga, E., Chateauneuf, A., Sánchez-Silva, M., Bressolette, P., Schoefs, F., 2010. Influence of
794 weather and global warming in chloride ingress into concrete: A stochastic approach. Structural Safety
795 32 (4), 238-249.

796 Bertolini, L., Elsener, B., Pedeferri, P., Redaelli, E., Polder, R.B., 2013. Corrosion of steel in concrete:
797 prevention, diagnosis, repair. John Wiley & Sons.
798 Cai, R., Hu, Y., Yu, M., Liao, W., Yang, L., Kumar, A., Ma, H., 2020. Skin effect of chloride ingress in
799 marine concrete: A review on the convection zone. Construction and Building Materials 262, 120566.
800 Cao, J., Jin, Z., Ding, Q., Xiong, C., Zhang, G., 2022. Influence of the dry/wet ratio on the chloride
801 convection zone of concrete in a marine environment. Construction and Building Materials 316,
802 125794.
803 Cao, Y., Gehlen, C., Angst, U., Wang, L., Wang, Z., Yao, Y., 2019. Critical chloride content in reinforced
804 concrete—An updated review considering Chinese experience. Cement and Concrete Research 117,
805 58-68.
806 Care, S., 2008. Effect of temperature on porosity and on chloride diffusion in cement pastes. Construction
807 and Building Materials 22 (7), 1560-1573.
808 Carsana, M., Gastaldi, M., Redaelli, E., 2022. A case study on corrosion conditions and guidelines for repair
809 of a reinforced concrete chimney in industrial environment. Structure and Infrastructure Engineering
810 19 (3), 366-377.
811 Chalhoub, C., Francois, R., Carcasses, M., 2020. Effect of cathode–anode distance and electrical resistivity
812 on macrocell corrosion currents and cathodic response in cases of chloride induced corrosion in
813 reinforced concrete structures. Construction and Building Materials 245, 118337.
814 Chang, H., 2017. Chloride binding capacity of pastes influenced by carbonation under three conditions.
815 Cement and Concrete Composites 84, 1-9.
816 Chang, H., Mu, S., Feng, P., 2018. Influence of carbonation on “maximum phenomenon” in surface layer
817 of specimens subjected to cyclic drying-wetting condition. Cement and Concrete Research 103, 95-109.
818 Chang, H., Mu, S., Xie, D., Wang, P., 2017. Influence of pore structure and moisture distribution on chloride
819 “maximum phenomenon” in surface layer of specimens exposed to cyclic drying-wetting condition.
820 Construction and Building Materials 131, 16-30.
821 Chen, C., Wang, L., Liu, R., Zhu, P., Liu, H., Wang, X., Yu, J., Chen, Y., 2023. Chloride penetration of
822 concrete exposed to dry-wet cycle with various dry-wet ratios and temperature. Construction and
823 Building Materials 400, 132883.

824 Chen, J.J., Thomas, J.J., Jennings, H.M., 2006. Decalcification shrinkage of cement paste. Cement and
825 Concrete Research 36 (5), 801-809.
826 Chen, L., Su, R.K.L., 2020. Effect of high rebar temperature during casting on corrosion in carbonated
827 concrete. Construction and Building Materials 249, 118718.
828 Chen, L., Su, R.K.L., 2023. Experimental and numerical investigations on macrocell corrosion of partially
829 carbonated reinforced concrete with supplementary cementitious materials. Cement and Concrete
830 Composites 135, 104827.
831 Costa, A., Appleton, J., 1999. Chloride penetration into concrete in marine environment—Part I: Main
832 parameters affecting chloride penetration. Materials and Structures 32, 252-259.
833 Criado, M., Provis, J.L., 2018. Alkali activated slag mortars provide high resistance to chloride-induced
834 corrosion of steel. Frontiers in Materials 5, 34.
835 Das, C.S., Zheng, H., Zhao, X.-L., Dai, J.-G., 2023. Corrosion inhibition of steel reinforcements in seawater
836 sea sand concrete by alkali-activated slag based coatings. Construction and Building Materials 394,
837 132210.
838 de Medeiros-Junior, R.A., de Lima, M.G., de Brito, P.C., de Medeiros, M.H.F., 2015. Chloride penetration
839 into concrete in an offshore platform-analysis of exposure conditions. Ocean Engineering 103, 78-87.
840 De Weerdt, K., Plusquellec, G., Revert, A.B., Geiker, M., Lothenbach, B., 2019. Effect of carbonation on
841 the pore solution of mortar. Cement and Concrete Research 118, 38-56.
842 Dehwah, H., Maslehuddin, M., Austin, S., 2003. Effect of sulfate ions and associated cation type on the
843 pore solution chemistry in chloride-contaminated plain and blended cements. Cement and Concrete
844 Composites 25 (4-5), 513-525.
845 Deus, J., Freire, L., Montemor, M., Nóvoa, X., 2012. The corrosion potential of stainless steel rebars in
846 concrete: Temperature effect. Corrosion Science 65, 556-560.
847 Dhir, R., Jones, M., Elghaly, A., 1993. PFA concrete: Exposure temperature effects on chloride diffusion.
848 Cement and Concrete Research 23 (5), 1105-1114.
849 Díaz, B., Guitián, B., Nóvoa, X., Pérez, M., 2018. The effect of long-term atmospheric aging and
850 temperature on the electrochemical behaviour of steel rebars in mortar. Corrosion Science 140, 143-
851 150.

852 Dousti, A., Khaksar, H., 2023. Impact of Simultaneous Carbonation and Chloride Attack on Chloride
853 Diffusion in Portland Cement Concrete Mixtures Blended with Natural Zeolite and Silica Fume. Journal
854 of materials in civil engineering 35 (12), 04023478.
855 Dousti, A., Rashetnia, R., Ahmadi, B., Shekarchi, M., 2013. Influence of exposure temperature on chloride
856 diffusion in concretes incorporating silica fume or natural zeolite. Construction and Building Materials
857 49, 393-399.
858 Dousti, A., Shekarchi, M., 2015. Effect of exposure temperature on chloride-binding capacity of cementing
859 materials. Magazine of Concrete Research 67 (15), 821-832.
860 El Hassan, J., Bressolette, P., Chateauneuf, A., El Tawil, K., 2010. Reliability-based assessment of the
861 effect of climatic conditions on the corrosion of RC structures subject to chloride ingress. Engineering
862 Structures 32 (10), 3279-3287.
863 Feliu, S., Morcillo, M., Chico, B., 1999. Effect of distance from sea on atmospheric corrosion rate.
864 Corrosion 55 (9), 883-891.
865 Feng, X., Wu, T., Luo, J.-l., Lu, X., 2020. Degradation of passive film on 304 stainless steel in a simulated
866 concrete pore solution under alternating temperature condition. Cement and Concrete Composites 112,
867 103651.
868 Figueira, R.B., Sadovski, A., Melo, A.P., Pereira, E.V., 2017. Chloride threshold value to initiate
869 reinforcement corrosion in simulated concrete pore solutions: The influence of surface finishing and
870 pH. Construction and Building Materials 141, 183-200.
871 Florea, M., Brouwers, H., 2012. Chloride binding related to hydration products: Part I: Ordinary Portland
872 Cement. Cement and Concrete Research 42 (2), 282-290.
873 Gang, X., Yun-pan, L., Yi-biao, S., Ke, X., 2015. Chloride ion transport mechanism in concrete due to
874 wetting and drying cycles. Structural Concrete 16 (2), 289-296.
875 Gastaldi, M., Bertolini, L., 2014. Effect of temperature on the corrosion behaviour of low-nickel duplex
876 stainless steel bars in concrete. Cement and Concrete Research 56, 52-60.
877 Geng, J., Easterbrook, D., Liu, Q.-F., Li, L.-Y., 2016. Effect of carbonation on release of bound chlorides
878 in chloride-contaminated concrete. Magazine of Concrete Research 68 (7), 353-363.

879 Guo, H., Dong, Y., Gu, X., 2020. Durability assessment of reinforced concrete structures considering global
880 warming: A performance-based engineering and experimental approach. Construction and Building
881 Materials 233, 117251.
882 Guzman, R.S., Vilche, J.R., Arvia, A.J., 1979. The potentiodynamic behaviour of iron in alkaline solutions.
883 Electrochimica Acta 24 (4), 395-403.
884 Hay, R., Celik, K., 2024. Comparative performance of OPC and LC3-based composites under combined
885 action of carbonation and chloride exposure. Construction and Building Materials 429, 136428.
886 Holthuizen, P.E., Çopuroğlu, O., Polder, R.B., 2018. Chloride ingress of carbonated blast furnace slag
887 cement mortars, High Tech Concrete: Where Technology and Engineering Meet. Springer, pp. 73-82.
888 Hong, K., Hooton, R., 1999. Effects of cyclic chloride exposure on penetration of concrete cover. Cement
889 and Concrete Research 29 (9), 1379-1386.
890 Hooton, R.D., 2019. Future directions for design, specification, testing, and construction of durable concrete
891 structures. Cement and Concrete Research 124, 105827.
892 Huet, B., L'Hostis, V., Miserque, F., Idrissi, H., 2005. Electrochemical behavior of mild steel in concrete:
893 Influence of pH and carbonate content of concrete pore solution. Electrochimica Acta 51 (1), 172-180.
894 Hussain, R.R., Ishida, T., 2010. Influence of connectivity of concrete pores and associated diffusion of
895 oxygen on corrosion of steel under high humidity. Construction and Building Materials 24 (6), 1014-
896 1019.
897 Hussain, S.E., 1993. Effect of temperature on pore solution composition in plain cements. Cement and
898 Concrete Research 23 (6), 1357-1368.
899 Isteita, M., Xi, Y., 2017. The effect of temperature variation on chloride penetration in concrete.
900 Construction and Building Materials 156, 73-82.
901 Jaśniok, T., Jaśniok, M., 2015. Influence of rapid changes of moisture content in concrete and temperature
902 on corrosion rate of reinforcing steel. Procedia Engineering 108, 316-323.
903 Jiang, J.-h., Yuan, Y.-s., 2013. Development and prediction strategy of steel corrosion rate in concrete under
904 natural climate. Construction and Building Materials 44, 287-292.

905 Jin, H., Fan, X., Li, Z., Zhang, W., Liu, J., Zhong, D., Tang, L., 2022. An experimental study on the
906 influence of continuous ambient humidity conditions on relative humidity changes, chloride diffusion
907 and microstructure in concrete. Journal of Building Engineering 59, 105112.
908 Jin, H., Liu, J., Jiang, Z., Zhou, H., Liu, J., 2021. Influence of the rainfall intensity on the chloride ion
909 distribution in concrete with different levels of initial water saturation. Construction and Building
910 Materials 281, 122561.
911 Jin, H., Liu, J., Zhong, D., Tang, L., 2023. Experimental study on chloride ion diffusion behavior and
912 microstructure in concrete under alternating ambient humidity conditions. Construction and Building
913 Materials 401, 132886.
914 Jin, M., Gao, S., Jiang, L., Chu, H., Lu, M., Zhi, F.F., 2018. Degradation of concrete with addition of
915 mineral admixture due to free chloride ion penetration under the effect of carbonation. Corrosion
916 Science 138, 42-53.
917 Ju, X., Wu, L., Lin, C., Yang, X., Yang, C., 2021. Prediction of chloride concentration with elevation in
918 concrete exposed to cyclic drying-wetting conditions in marine environments. Construction and
919 Building Materials 278, 122370.
920 Justnes, H., Skocek, J., Østnor, T.A., Engelsen, C.J., Skjølsvold, O., 2020. Microstructural changes of
921 hydrated cement blended with fly ash upon carbonation. Cement and Concrete Research 137, 106192.
922 Kuosa, H., Ferreira, R., Holt, E., Leivo, M., Vesikari, E., 2014. Effect of coupled deterioration by freeze–
923 thaw, carbonation and chlorides on concrete service life. Cement and Concrete Composites 47, 32-40.
924 Li, B., Giordano, R., Tulliani, J.-M., Meng, Q., 2024. Effect of sea salt on carbonation and CO2 uptake in
925 cement mortar. Construction and Building Materials 438, 137212.
926 Li, B., Huan, Y., Zhang, W., 2017. Passivation and corrosion behavior of P355 carbon steel in simulated
927 concrete pore solution at pH 12.5 to 14. Int. J. Electrochem. Sci 12, 10402-10420.
928 Li, C.-z., Song, X.-b., 2022. Mesoscale modeling of chloride transport in unsaturated concrete based on
929 Voronoi tessellation. Cement and Concrete Research 161, 106932.
930 Li, J., Shao, W., 2014. The effect of chloride binding on the predicted service life of RC pipe piles exposed
931 to marine environments. Ocean Engineering 88, 55-62.

Li, J., Xiong, J., Fan, Z., Chen, M., Sun, L., Zhu, C., Liu, W., Zheng, H., Li, W., 2023a. Mechanistic study of macrocell effect on corrosion initiation and propagation of reinforcement in submarine immersed tunnel. Cement and Concrete Composites 136, 104890.

Li, J., Xiong, J., Fan, Z., Gu, Z., Chen, M., Sun, L., Zheng, H., Li, W., 2023b. Macrocell Effect on Chloride Threshold Value and Corrosion Rate of Steel Bar in Simulated Concrete Pore Solution. Journal of materials in civil engineering 35 (12), 04023436.

Li, K., Zhang, Y., Wang, S., Zeng, J., 2018. Impact of carbonation on the chloride diffusivity in concrete: experiment, analysis and application. Materials and Structures 51 (6), 1-15.

Liang, C., Cai, Z., Wu, H., Xiao, J., Zhang, Y., Ma, Z., 2021. Chloride transport and induced steel corrosion in recycled aggregate concrete: A review. Construction and Building Materials 282, 122547.

Lindvall, A., 2007. Chloride ingress data from field and laboratory exposure–Influence of salinity and temperature. Cement and Concrete Composites 29 (2), 88-93.

Liu, J.-z., Ba, M.-f., Du, Y.-g., He, Z.-m., Chen, J.-b., 2016a. Effects of chloride ions on carbonation rate of hardened cement paste by X-ray CT techniques. Construction and Building Materials 122, 619-627.

Liu, J., Ou, G., Qiu, Q., Xing, F., Tang, K., Zeng, J., 2018. Atmospheric chloride deposition in field concrete at coastal region. Construction and Building Materials 190, 1015-1022.

Liu, J., Qiu, Q., Chen, X., Wang, X., Xing, F., Han, N., He, Y., 2016b. Degradation of fly ash concrete under the coupled effect of carbonation and chloride aerosol ingress. Corrosion Science 112, 364-372.

Liu, J., Qiu, Q., Chen, X., Xing, F., Han, N., He, Y., Ma, Y., 2017a. Understanding the interacted mechanism between carbonation and chloride aerosol attack in ordinary Portland cement concrete. Cement and Concrete Research 95, 217-225.

Liu, M., Cheng, X., Li, X., Zhou, C., Tan, H., 2017b. Effect of carbonation on the electrochemical behavior of corrosion resistance low alloy steel rebars in cement extract solution. Construction and Building Materials 130, 193-201.

Liu, P., Yu, Z., Lu, Z., Chen, Y., Liu, X., 2016c. Predictive convection zone depth of chloride in concrete under chloride environment. Cement and Concrete Composites 72, 257-267.

Liu, R., Jiang, L., Huang, G., Zhu, Y., Liu, X., Chu, H., Xiong, C., 2016d. The effect of carbonate and sulfate ions on chloride threshold level of reinforcement corrosion in mortar with/without fly ash. Construction and Building Materials 113, 90-95.

Liu, R., Jiang, L., Xu, J., Xiong, C., Song, Z., 2014. Influence of carbonation on chloride-induced reinforcement corrosion in simulated concrete pore solutions. Construction and Building Materials 56, 16-20.

Liu, T., Weyers, R., 1998. Modeling the dynamic corrosion process in chloride contaminated concrete structures. Cement and Concrete Research 28 (3), 365-379.

Liu, X., MacDonald, D.D., Wang, M., Xu, Y., 2021. Effect of dissolved oxygen, temperature, and pH on polarization behavior of carbon steel in simulated concrete pore solution. Electrochimica Acta 366, 137437.

Lothenbach, B., Scrivener, K., Hooton, R., 2011. Supplementary cementitious materials. Cement and Concrete Research 41 (12), 1244-1256.

Lu, C.-f., Wang, W., Jiang, J.-h., Hao, M., 2017. Micro-environment temperature and relative humidity response of fly ash concrete under natural climatic conditions. Advances in cement research 29 (6), 236-245.

Lu, C., Gao, Y., Cui, Z., Liu, R., 2015. Experimental analysis of chloride penetration into concrete subjected to drying–wetting cycles. Journal of materials in civil engineering 27 (12), 04015036.

Malheiro, R., Camões, A., Meira, G., Amorim, M.T., 2021. Influence of chloride contamination on carbonation of cement-based materials. Construction and Building Materials 296, 123756.

Malheiro, R., Camões, A., Meira, G., Amorim, M.T., Castro-Gomes, J., 2020. Effect of coupled deterioration by chloride and carbonation on chloride ions transport in concrete. RILEM Technical Letters 5, 56-62.

Maslehuddin, M., Paget, C., Rasheeduzzafar, 1997. Temperature effect on the pore solution chemistry in contaminated cements. Magazine of Concrete Research 49 (178), 5-14.

Medeiros-Junior, R.A., 2018. Impact of climate change on the service life of concrete structures, Eco-efficient repair and rehabilitation of concrete infrastructures. Elsevier, pp. 43-68.

985 Medeiros, M., Gobbi, A., Réus, G., Helene, P., 2013. Reinforced concrete in marine environment: Effect
986 of wetting and drying cycles, height and positioning in relation to the sea shore. Construction and
987 Building Materials 44, 452-457.
988 Meira, G.R., Andrade, C., Alonso, C., Borba Jr, J., Padilha Jr, M., 2010. Durability of concrete structures
989 in marine atmosphere zones–The use of chloride deposition rate on the wet candle as an environmental
990 indicator. Cement and Concrete Composites 32 (6), 427-435.
991 Meira, G.R., Andrade, C., Alonso, C., Padaratz, I., Borba Jr, J., 2007a. Salinity of marine aerosols in a
992 Brazilian coastal area—Influence of wind regime. Atmospheric environment 41 (38), 8431-8441.
993 Meira, G.R., Andrade, C., Alonso, C., Padaratz, I., Borba, z.J., 2008. Modelling sea-salt transport and
994 deposition in marine atmosphere zone–A tool for corrosion studies. Corrosion Science 50 (9), 2724-
995 2731.
996 Meira, G.R., Andrade, C., Padaratz, I., Alonso, C., Borba Jr, J., 2007b. Chloride penetration into concrete
997 structures in the marine atmosphere zone–Relationship between deposition of chlorides on the wet
998 candle and chlorides accumulated into concrete. Cement and Concrete Composites 29 (9), 667-676.
999 Meira, G.R., Andrade, M., Padaratz, I., Alonso, M.C., Borba Jr, J., 2006. Measurements and modelling of
1000 marine salt transportation and deposition in a tropical region in Brazil. Atmospheric environment 40
1001 (29), 5596-5607.
1002 Melchers, R.E., 2020. Long-term durability of marine reinforced concrete structures. Journal of Marine
1003 Science and Engineering 8 (4), 290.
1004 Melchers, R.E., Chaves, I.A., 2020. Reinforcement corrosion in marine concretes-2. long-term effects. ACI
1005 materials journal 117 (2), 217-228.
1006 Melchers, R.E., Pape, T.M., Chaves, I.A., Heywood, R.J., 2017. Long-term durability of reinforced concrete
1007 piles from the Hornibrook Highway bridge. Australian journal of structural engineering 18 (1), 41-57.
1008 Moradllo, M.K., Sadati, S., Shekarchi, M., 2018. Quantifying maximum phenomenon in chloride ion
1009 profiles and its influence on service-life prediction of concrete structures exposed to seawater tidal
1010 zone–A field oriented study. Construction and Building Materials 180, 109-116.
1011 Morcillo, M., Chico, B., Mariaca, L., Otero, E., 2000. Salinity in marine atmospheric corrosion: its
1012 dependence on the wind regime existing in the site. Corrosion Science 42 (1), 91-104.

1013 Mundra, S., Provis, J.L., 2021. Mechanisms of passivation and chloride-induced corrosion of mild steel in
1014 sulfide-containing alkaline solutions. Journal of Materials Science, 1-20.
1015 Ngala, V., Page, C., 1997. Effects of carbonation on pore structure and diffusional properties of hydrated
1016 cement pastes. Cement and Concrete Research 27 (7), 995-1007.
1017 Nguyen, T., Lorente, S., Carcasses, M., 2009. Effect of the environment temperature on the chloride
1018 diffusion through CEM-I and CEM-V mortars: An experimental study. Construction and Building
1019 Materials 23 (2), 795-803.
1020 Ogirigbo, O.R., Black, L., 2017. Chloride binding and diffusion in slag blends: Influence of slag
1021 composition and temperature. Construction and Building Materials 149, 816-825.
1022 Otieno, M., Golden, G., Alexander, M., Beushausen, H., 2019. Acceleration of steel corrosion in concrete
1023 by cyclic wetting and drying: Effect of drying duration and concrete quality. Materials and Structures
1024 52 (2), 50.
1025 Page, C., 1975. Mechanism of corrosion protection in reinforced concrete marine structures. nature 258
1026 (5535), 514-515.
1027 Page, C., Short, N., El Tarras, A., 1981. Diffusion of chloride ions in hardened cement pastes. Cement and
1028 Concrete Research 11 (3), 395-406.
1029 Panesar, D., Chidiac, S., 2011. Effect of cold temperature on the chloride-binding capacity of cement.
1030 Journal of Cold Regions Engineering 25 (4), 133-144.
1031 Pati, A.R., 2010. Effects of rebar temperature and water to cement ratio on rebar-concrete bond strength of
1032 concrete containing fly ash. University of North Texas.
1033 Pergola, A.D., Lollini, F., Redaelli, E., Bertolini, L., 2013. Numerical modeling of initiation and
1034 propagation of corrosion in hollow submerged marine concrete structures. Corrosion 69 (12), 1158-
1035 1170.
1036 Pour-Ghaz, M., Isgor, O.B., Ghods, P., 2009a. The effect of temperature on the corrosion of steel in
1037 concrete. Part 1: Simulated polarization resistance tests and model development. Corrosion Science 51
1038 (2), 415-425.
1039 Pour-Ghaz, M., Isgor, O.B., Ghods, P., 2009b. The effect of temperature on the corrosion of steel in
1040 concrete. Part 2: Model verification and parametric study. Corrosion Science 51 (2), 426-433.

1041 Poursaee, A., 2016. Temperature dependence of the formation of the passivation layer on carbon steel in
1042 high alkaline environment of concrete pore solution. Electrochemistry Communications 73, 24-28.
1043 Poursaee, A., Hansson, C., 2007. Reinforcing steel passivation in mortar and pore solution. Cement and
1044 Concrete Research 37 (7), 1127-1133.
1045 Qiu, Q., 2020. A state-of-the-art review on the carbonation process in cementitious materials: Fundamentals
1046 and characterization techniques. Construction and Building Materials 247, 118503.
1047 Raupach, M., 1996a. Investigations on the influence of oxygen on corrosion of steel in concrete—Part 2.
1048 Materials and Structures 29, 226-232.
1049 Raupach, M., 1996b. Investigations on the influence of oxygen on corrosion of steel in concrete—Part I.
1050 Materials and Structures 29, 174-184.
1051 Revert, A.B., Hornbostel, K., De Weerdt, K., Geiker, M.R., 2019. Macrocell corrosion in carbonated
1052 Portland and Portland-fly ash concrete-Contribution and mechanism. Cement and Concrete Research
1053 116, 273-283.
1054 Ruan, T., Spandley, N., Johnson, C., Poursaee, A., 2015. The impact of fire and fire extinguishing method
1055 on the corrosion behavior of the steel bars in concrete pore solution. Fire Safety Journal 78, 196-201.
1056 Saillio, M., Baroghel-Bouny, V., Barberon, F., 2014. Chloride binding in sound and carbonated
1057 cementitious materials with various types of binder. Construction and Building Materials 68, 82-91.
1058 Saillio, M., Baroghel-Bouny, V., Bertin, M., Pradelle, S., Vincent, J., 2019. Phase assemblage of cement
1059 pastes with SCM at different ages. Construction and Building Materials 224, 144-157.
1060 Saillio, M., Baroghel-Bouny, V., Pradelle, S., Bertin, M., Vincent, J., de Lacaillerie, J.-B.d.E., 2021. Effect
1061 of supplementary cementitious materials on carbonation of cement pastes. Cement and Concrete
1062 Research 142, 106358.
1063 Samson, E., Marchand, J., 2007. Modeling the effect of temperature on ionic transport in cementitious
1064 materials. Cement and Concrete Research 37 (3), 455-468.
1065 Sánchez-Moreno, M., Takenouti, H., García-Jareño, J., Vicente, F., Alonso, C., 2009. A theoretical
1066 approach of impedance spectroscopy during the passivation of steel in alkaline media. Electrochimica
1067 Acta 54 (28), 7222-7226.

1068 Santhanam, M., Otieno, M., 2016. Deterioration of concrete in the marine environment. Marine concrete
1069 structures, 137-149.
1070 Segura, I., Cavalaro, S., Fuente, A.d.l., Aguado, A., Alegre, V., 2016. Service-life assessment of existing
1071 precast concrete structure exposed to severe marine conditions. Journal of Performance of Constructed
1072 Facilities 30 (3), 04015036.
1073 Shafikhani, M., Chidiac, S., 2019. Quantification of concrete chloride diffusion coefficient–A critical
1074 review. Cement and Concrete Composites 99, 225-250.
1075 Sharifi-Asl, S., Mao, F., Lu, P., Kursten, B., Macdonald, D.D., 2015. Exploration of the effect of chloride
1076 ion concentration and temperature on pitting corrosion of carbon steel in saturated Ca (OH) 2 solution.
1077 Corrosion Science 98, 708-715.
1078 Shi, J., Wu, M., Ming, J., 2020. Degradation effect of carbonation on electrochemical behavior of 2304
1079 duplex stainless steel in simulated concrete pore solutions. Corrosion Science 177, 109006.
1080 Shi, X., Xie, N., Fortune, K., Gong, J., 2012. Durability of steel reinforced concrete in chloride
1081 environments: An overview. Construction and Building Materials 30, 125-138.
1082 Song, H.-W., Lee, C.-H., Ann, K.Y., 2008. Factors influencing chloride transport in concrete structures
1083 exposed to marine environments. Cement and Concrete Composites 30 (2), 113-121.
1084 Spragg, R.P., Castro, J., Li, W., Pour-Ghaz, M., Huang, P.-T., Weiss, J., 2011. Wetting and drying of
1085 concrete using aqueous solutions containing deicing salts. Cement and Concrete Composites 33 (5),
1086 535-542.
1087 Stefanoni, M., Angst, U., Elsener, B., 2020. The mechanism controlling corrosion of steel in carbonated
1088 cementitious materials in wetting and drying exposure. Cement and Concrete Composites 113, 103717.
1089 Stewart, M.G., Wang, X., Nguyen, M.N., 2011. Climate change impact and risks of concrete infrastructure
1090 deterioration. Engineering Structures 33 (4), 1326-1337.
1091 Thomas, M., Hooton, R., Scott, A., Zibara, H., 2012. The effect of supplementary cementitious materials
1092 on chloride binding in hardened cement paste. Cement and Concrete Research 42 (1), 1-7.
1093 Tongning, C., Lijuan, Z., Guowen, S., Caihui, W., Ying, Z., Pengshuo, W., Aoxue, X., 2020. Simulation of
1094 chloride ion transport in concrete under the coupled effects of a bending load and drying–wetting cycles.
1095 Construction and Building Materials 241, 118045.

Tran, V.Q., Nguyen, H.-L., Dao, D.V., Hilloulin, B., Nguyen, L.K., Nguyen, Q.H., Le, T.-T., Ly, H.-B., 2021. Effect of temperature on the chloride binding capacity of cementitious materials. Magazine of Concrete Research 73 (15), 771-784.

von Greve-Dierfeld, S., Lothenbach, B., Vollpracht, A., Wu, B., Huet, B., Andrade, C., Medina, C., Thiel, C., Gruyaert, E., Vanoutrive, H., 2020. Understanding the carbonation of concrete with supplementary cementitious materials: a critical review by RILEM TC 281-CCC. Materials and Structures 53 (6), 1-34.

Wang, D., Wu, J., Wang, Q., Wan, L., Emori, W., Zhang, S., Wang, J., 2021. Temperature-dependent corrosion behaviour of the amorphous steel in simulated wet storage environment of spent nuclear fuels. Corrosion Science 188, 109529.

Wang, S., Liu, D., Du, N., Zhao, Q., Xiao, J., 2016. Cathodic reactions involved in the corrosion of X80 steel in acidic soil simulated solution. Int. J. Electrochem. Sci 11, 8797-8809.

Wang, Y., Nanukuttan, S., Bai, Y., Basheer, P., 2017. Influence of combined carbonation and chloride ingress regimes on rate of ingress and redistribution of chlorides in concretes. Construction and Building Materials 140, 173-183.

Wu, B., Ye, G., 2017. Development of porosity of cement paste blended with supplementary cementitious materials after carbonation. Construction and Building Materials 145, 52-61.

Wu, L., Wang, W., Jiang, C., 2023. Study on the similarity of chloride penetration in concrete exposed to field and laboratory conditions. Materials and Structures 56 (5), 95.

Xie, X., Feng, Q., Chen, Z., Jiang, L., Lu, W., 2019. Diffusion and distribution of chloride ions in carbonated concrete with fly ash. Construction and Building Materials 218, 119-125.

Xie, Y., Xie, J., Bai, L., Liu, J., 2023. Experimental study on the effect of salt on the water absorption characteristic of cement mortar. Journal of Building Engineering 73, 106693.

Xu, J., Song, Y., Jiang, L., Feng, W., Cao, Y., Ji, W., 2016. Influence of elevated temperature on release of bound chlorides from chloride-admixed plain and blended cement pastes. Construction and Building Materials 104, 9-15.

Ye, H., Jin, X., Fu, C., Jin, N., Xu, Y., Huang, T., 2016. Chloride penetration in concrete exposed to cyclic drying-wetting and carbonation. Construction and Building Materials 112, 457-463.

1124 Yi, Y., Zhu, D., Guo, S., Zhang, Z., Shi, C., 2020. A review on the deterioration and approaches to enhance
1125 the durability of concrete in the marine environment. Cement and Concrete Composites 113, 103695.
1126 Yoon, I.S., 2007. Deterioration of concrete due to combined reaction of carbonation and chloride
1127 penetration: experimental study. Key Engineering Materials 348, 729-732.
1128 Yuan, Q., Shi, C., De Schutter, G., Audenaert, K., 2008. Effect of temperature on transport of chloride ions
1129 in concrete, Concrete repair, rehabilitation and retrofitting II. CRC Press, pp. 177-178.
1130 Zha, J., Jiang, L., Xu, P., Jin, M., Jiang, P., 2022. Influence of Temperature and Carbonation on Chloride
1131 Induced Corrosion of Carbon Steel in Concrete Pore Solutions. Int. J. Electrochem. Sci 17 (220130), 2.
1132 Zhang, P., Dai, J.-G., Das, C.S., Zheng, J.-J., 2023a. A fully coupled meso-scale electro-chemo-mechanical
1133 phase field method for corrosion-induced fracture in concrete. International Journal of Solids and
1134 Structures 267, 112165.
1135 Zhang, Y., Wu, S., Zhang, Y., Zhou, C., Fu, C., 2023b. Similarities and probability distributions of chloride
1136 convection zone depth in concrete exposed to cyclic drying-wetting environments. Cement and
1137 Concrete Composites 139, 105040.
1138 Zhang, Y., Zhang, M., 2014. Transport properties in unsaturated cement-based materials–A review.
1139 Construction and Building Materials 72, 367-379.
1140 Zheng, Y., Russell, M., Davis, G., McPolin, D., Yang, K., Basheer, P., Nanukuttan, S., 2021. Influence of
1141 carbonation on the bound chloride concentration in different cementitious systems. Construction and
1142 Building Materials 302, 124171.
1143 Zibara, H., 2001. Binding of external chlorides by cement pastes.
1144 Zuquan, J., Xia, Z., Tiejun, Z., Jianqing, L., 2018. Chloride ions transportation behavior and binding
1145 capacity of concrete exposed to different marine corrosion zones. Construction and Building Materials
1146 177, 170-183.

1147

1148

Table 1. Mix composition and testing condition for evaluating the nature of chloride transport in drying and wetting zones

Mix	Cement type	Supplementary cementitious materials (% wt replacement of cement)			W/b	Exposure scheme	Exposure period (d)	Ref
		FA	GGBS	SF				
#1	OPC	-	-	-	0.35	Field exposure in a marine tidal zone in Qingdao Wheat Island, China, for 12-hour cycles with three drying-to-wetting ratios of (i) 11:1, (ii) 1:1 and (iii) 1:11	30, 60, 90	(Cao et al., 2022)
#2	OPC	17	32	-	0.35			
#3	OPC	-	-	-	0.43	Drying and wetting cycles in a lab with 5% by weight NaCl solution for (i) 2-week cycle with 7 days wetting and 7 days drying (ii) 3-week cycle with 7 days wetting and 14 days drying	420	(Lu et al., 2015)
#4	OPC	-	-	-	0.385			
#5	OPC	15	-	-	0.385			
#6	OPC	30	-	-	0.385			

FA: Fly ash, GGBS: Ground granulated blast furnace slag, Sf: Silica fume

Table 2. Concrete mix and testing condition for evaluating the effect of temperature on chloride binding ability of cement paste

Mix	Cement type	Supplementary cementitious materials (% wt replacement of cement)				W/b	Exposure condition	Exposure temperature (°C)	Ref
		MK	GGBS	NZ	SF				
#1	OPC	-	-		-	0.4	25 g of powder samples cured for two months were exposed to 100 ml NaCl solutions of concentrations 0.1M, 0.5M, 1M, 2M, and 3M for eight weeks	-4, 3, 22, 35, 50, 70	(Dousti and Shekarchi, 2015)
#2	OPC	-	-	-	8	0.4			
#3	OPC	8	-	-	-	0.4			
#4	OPC	-	-	10	-	0.4			
#5	OPC	-	-	-	-	0.31	2.5-gram samples of size 10 X 10 X 2.5 mm thickness cured for 28 days were stored in 5 ml NaCl solutions of concentrations 0.1M, 0.5M, 0.75M, 1M, and 3M for 55 days	-3, 5, 13, 22	(Panesar and Chidiac, 2011)
#6	OPC	-	25	-	-	0.31			
#7	OPC	-	50	-	-	0.31			
#8	OPC	-	75	-	-	0.31			
#9	OPC	-	-	-	-	0.3, 0.5	25 gram of disc specimens of 50 mm diameter and 3 mm thickness cured for 9 months were placed in 125 ml NaCl solutions of concentrations 0.1M, 1M and 3M for 6 months	7, 23 and 38	(Zibara, 2001)
#10	OPC	-	-	-	8	0.3, 0.5			
#11	OPC	8	-	-	-	0.3, 0.5			

MK: Metakaolin, NZ: Natural pozzolona

Table 3. Concrete mix proportion and testing condition for evaluating the effect of temperature on chloride diffusion coefficient and activation energy

Mix	Cement type	Supplementary cementitious materials (% wt replacement of cement)				W/b	Exposure condition	Exposure temperature (°C)	Ref
		SF	FA	MK	NZ				
#1	OPC	-	-	-	-	0.35	Diffusion tests following NT Build 443 (165 g/l NaCl solution) were conducted on samples cured for 56 days for a period of 42 days	5, 25, 40	(Yuan et al., 2008)
#2	OPC	-	-	-	-	0.48			
#3	OPC	-	-	-	-	0.6			
#4	OPC	-	-	-	-	0.40	Concrete cylindrical samples of diameter 150 mm, which were cured for 5 months, were immersed in 32 g/l NaCl solution for a period of 450 days	22, 35, 50	(Dousti et al., 2013)
#5	OPC	5	-	-	-	0.40			
#6	OPC	10	-	-	-	0.40			
#7	OPC	12.5	-	-	-	0.40			
#8	OPC	-	-	-	10	0.40			
#9	OPC	-	-	-	15	0.40			

#10	OPC	-	-	-	20	0.40			
#11	OPC	-	-	-	-	0.4	75 mm diameter and 150 mm height samples, which were cured for 21 days before being immersed in 26 g/L of Cl solution for 365 days	22, 35, 50, 60	(Al-Sodani et al., 2021)
#12	OPC	-	20	-	-	0.4			
#13	CEMI	-	-	-		0.39	11 cm diameter and 5 cm thick cylinders were cured for 28 days after immersing in 33 g/L NaCl solution for 180 days		
#14	CEMV	-	-	-	-	0.43			
#15	OPC	-	-	-	-	0.38	75 mm diameter and 150 mm height samples, which were cured for 28 days before being immersed in 45 g/L of NaCl solution for 390 days	23, 38, 53, 68	(Al-Sodani, 2022)
#16	OPC	-	-	-	-	0.38			
#17	OPC	5	-	-	-	0.38			
#18	OPC	10	-	-	-	0.38			
#19	OPC	15	-	-	-	0.38			
#20	OPC	-	-	5	-	0.38			
#21	OPC	-	-	10	-	0.38			
#22	OPC	-	-	15	-	0.38			

Table 4. Mixing composition and testing parameters of studies involving effect of carbonation on chloride transport rate.

Mix	Cement type	Supplementary cementitious materials (% wt replacement of cement)			CO_2 conc	CO_2 exposure period (d)	W/b	Chloride transport testing method	Chloride ingress testing starting age (d)	Ref
		FA	GGBS	SF						
#1	OPC	-	-	-	5%	90	0.55	Immersion for 3 months as per NT Build 443	150	(Wang et al., 2017)
#2	OPC	30	-	-	5%	90	0.55		150	
#3	OPC	10	-	5	5%	90	0.55		150	
#4	OPC	-	-	-	20%	28	0.38	10h aerosol chloride spray and 14h drying for 28 days	56	(Liu et al., 2017a)
#5	OPC	-	-	-	20%	28	0.47		56	
#6	OPC	-	-	-	20%	28	0.53		56	

#7	OPC	-	-	-	20%	28	0.47	10h aerosol chloride spray and 14h drying for 28 days	56	(Liu et al., 2016b)
#8	OPC	15	-	-	20%	28	0.47		56	
#9	OPC	30	-	-	20%	28	0.47		56	
#10	OPC	-	-	-	20%	62	0.51	Use of empirical equation to obtain chloride diffusion coefficient from ASTM C1202	90	(Xie et al., 2019)
#11	OPC	15	-	-	20%	62	0.57		90	
#12	OPC	30	-	-	20%	62	0.53		90	
#13	OPC	-	-	-	20%	62	0.35		90	
#14	OPC	15	-	-	20%	62	0.33		90	
#15	OPC	30	-	-	20%	62	0.26		90	
#16	CEM I 42.5R	-	-	-	4%	30	0.60	Non steady migration test as per LNEC	150	(Malheiro et al., 2020)
#17	CEM I 42.5R	-	-	-	4%	210	0.60		330	
#18	OPC PO42.5	-	-	-	20%	90	0.5		180	
#19	OPC PO42.5	-	-	-	20%	90	0.6		180	

#20	OPC PO42.5	8.6	7.6	-	20%	90	0.5	Immersion for 35 days as per NT Build 443	180	(Li et al., 2018)
#21	OPC PO42.5	14.7	12.9	-	20%	90	0.6		180	
#22	OPC PII 42.5	-	-	-	20%	28	0.35	Immersion in 1M/litre NaCl solution for 6 weeks (diffusion coefficient of free chlorides only)	56	(Jin et al., 2018)
#23	OPC PII 42.5			-	20%	28	0.45		56	
#24	OPC PII 42.5	-	-	-	20%	28	0.55		56	
#25	OPC PII 42.5	34.9	-	-	20%	28	0.55		56	
#26	OPC PII 42.5	-	34.9	-	20%	28	0.55		56	
#27	CEM I	-	-	-	3%	180	0.5		208	
#28	CEM I	-	20	-	3%	180	0.5		208	
#29	CEM I	-	25	-	3%	180	0.5		208	
#30	CEM I	-	30	-	3%	180	0.5		208	
#31	CEM I	-	35	-	3%	180	0.5		208	
#32	CEM I	-	40	-	3%	180	0.5		208	

#33	CEM I	-	45	-	3%	180	0.5	NT Build 492	208	(Holthuizen et al., 2018)
#34	CEM I	-	50	-	3%	180	0.5		208	
#35	CEM I	-	55	-	3%	180	0.5		208	
#36	CEM I	-	60	-	3%	180	0.5		208	
#37	CEM I	-	65	-	3%	180	0.5		208	
#38	CEM I	-	70	-	3%	180	0.5		208	

Al-Sodani, K.A.A., 2022. Effect of exposure temperatures on chloride penetration resistance of concrete incorporating polypropylene Fibers, silica fume and metakaolin. Construction and Building Materials 346, 128445.

Al-Sodani, K.A.A., Al-Zahrani, M.M., Maslehuddin, M., Al-Amoudi, O.S.B., Al-Dulaijan, S.U., 2021. Chloride diffusion models for Type I and fly ash cement concrete exposed to field and laboratory conditions. Marine Structures 76, 102900.

Cao, J., Jin, Z., Ding, Q., Xiong, C., Zhang, G., 2022. Influence of the dry/wet ratio on the chloride convection zone of concrete in a marine environment. Construction and Building Materials 316, 125794.

Dousti, A., Rashetnia, R., Ahmadi, B., Shekarchi, M., 2013. Influence of exposure temperature on chloride diffusion in concretes incorporating silica fume or natural zeolite. Construction and Building Materials 49, 393-399.

Dousti, A., Shekarchi, M., 2015. Effect of exposure temperature on chloride-binding capacity of cementing materials. Magazine of Concrete Research 67 (15), 821-832.

Holthuizen, P.E., Çopuroğlu, O., Polder, R.B., 2018. Chloride ingress of carbonated blast furnace slag cement mortars, High Tech Concrete: Where Technology and Engineering Meet. Springer, pp. 73-82.

Jin, M., Gao, S., Jiang, L., Chu, H., Lu, M., Zhi, F.F., 2018. Degradation of concrete with addition of mineral admixture due to free chloride ion penetration under the effect of carbonation. Corrosion Science 138, 42-53.

Li, K., Zhang, Y., Wang, S., Zeng, J., 2018. Impact of carbonation on the chloride diffusivity in concrete: experiment, analysis and application. Materials and Structures 51 (6), 1-15.

Liu, J., Qiu, Q., Chen, X., Wang, X., Xing, F., Han, N., He, Y., 2016. Degradation of fly ash concrete under the coupled effect of carbonation and chloride aerosol ingress. Corrosion Science 112, 364-372.

Liu, J., Qiu, Q., Chen, X., Xing, F., Han, N., He, Y., Ma, Y., 2017. Understanding the interacted mechanism between carbonation and chloride aerosol attack in ordinary Portland cement concrete. Cement and Concrete Research 95, 217-225.

Lu, C., Gao, Y., Cui, Z., Liu, R., 2015. Experimental analysis of chloride penetration into concrete subjected to drying–wetting cycles. Journal of materials in civil engineering 27 (12), 04015036.

Malheiro, R., Camões, A., Meira, G., Amorim, M.T., Castro-Gomes, J., 2020. Effect of coupled deterioration by chloride and carbonation on chloride ions transport in concrete. RILEM Technical Letters 5, 56-62.